Investigating the Influence of Nanotopography on the Migratory State of Glioblastoma Multiforme Cells

A thesis submitted to the faculty of
Worcester Polytechnic Institute
In partial fulfillment of the requirements of the
Degree of Master of Science in Biomedical Engineering

Submitted by:

Alexander Beliveau

Approved by:

Anjana Jain, PhD
Assistant Professor
Department of Biomedical Engineering

Kristen Billiar, PhD
Professor
Department of Biomedical Engineering

Qi Wen, PhD
Assistant Professor
Department of Physics

Worcester Polytechnic Institute
January 20, 2016

ABSTRACT

Glioblastoma multiforme (GBM) is an aggressive Grade IV astrocytoma with a poor survival rate. This is largely due to the GBM tumor cells migrating away from the primary tumor site along white matter tracts and blood vessels leading to secondary tumor sites. It is unknown whether the microenvironment nanotopography influences the biomechanical properties of the tumor cells. Although these tumor cells have an innate propensity to migrate, we believe that the nanotopography changes the biomechanical properties to enhance the migratory phenotype. To study this, we used an *in vitro* polycaprolactone aligned nanofiber film that mimics the nanotopography of the white matter tracts and blood vessels to investigate the mechanical properties of the GBM tumor cells. Our data demonstrate that the cytoskeletal stiffness, traction force, and focal adhesion area are inherently lower in invasive GBM tumor cells compared to healthy astrocytes. Moreover, the tumor cytoskeletal stiffness was significantly reduced when cultured on the aligned nanofiber films compared to smooth and randomly aligned nanofibers films. Analysis of gene expression also showed that tumor cells cultured on the aligned nanotopography upregulated key migratory genes and downregulated key proliferative genes. In addition, cell cycle analysis exhibited a reduced proliferative state on aligned nanofibers, highlighting the dichotomy between proliferation and migration observed in GBM. Finally, focal adhesions of tumor cells were larger and more elliptical when grown on the aligned fibers, suggesting a more migratory state. Therefore, our data demonstrate that the invasive potential is elevated when the tumor cells are cultured on an aligned nanotopography. This *in vitro* model can further be used to identify the GBM tumor cells' response in a mimetic *in vivo* tumor microenvironment and elucidate how the aligned nanotopography transduces into altered gene and protein expression, thus providing a mechanism to target to inhibit the enhanced migratory behavior observed in these cells.

ACKNOWLEDGEMENTS

I would like to thank my advisor, Dr. Anjana Jain, for her motivation, critical discussions, and providing me the research space to complete this project. Her guidance and support has been invaluable for the completion of this project, and has given me the opportunity to learn and grow.

I would also like to thank the rest of my committee members, Dr. Kristen Billiar and Dr. Qi Wen, for their feedback, guidance, facilities, and discussions throughout this project.

I would also like to thank all of the graduate students and undergraduate volunteers of the Jain lab for teaching me lab techniques, providing a helpful hand, listening, and supporting me through the process.

I would also like to thank Gawain Thomas and Dr. Jiaxin Gong of the Wen lab for their tremendous help with the AFM and TFM, respectively. I would like to acknowledge Dr. Rosalind Segal (Dana-Farber Cancer Institute) and Dr. Ravi Bellamkonda (Georgia Institute of Technology) for generously providing us with BT145 and U87MG-eGFP tumor cells, respectively. I also sincerely appreciate Dr. Sakthikumar Ambady for his assistance in generating A172-GFP Actin cells, Victoria Huntress for her assistance with the confocal microscope, Dr. Robert Gegear for his assistance with statistical analysis, and Dr. Roger Ristau (University of Connecticut) and Anbo Wang for their assistance with the SEM. I would also like to thank the rest of the BME department at WPI.

Finally, I would like to thank my family and friends for their unwavering support and encouragement throughout my education.

TABLE OF CONTENTS

TABLE OF FIGURES

TABLE OF TABLES

CHAPTER 1: INTRODUCTION

Glioblastoma multiforme (GBM) is an aggressive malignant brain tumor that accounts for 45.6% of primary brain tumors [1]. Standard clinical treatments include surgical resection, chemotherapy, and radiation therapy. However, with a combination of these treatments, the average survival time is about 14.6 months [2]. Moreover, the recurrence rate remains high (~90%) due to the highly invasive nature of the GBM cells [3]. In addition, cancer initiating cells (CICs), a self-renewing subset of the heterogenic cell population, are highly migratory, invasive, and are responsible for recurrence of the tumor [4]. It has been shown that the GBM cells migrate and invade healthy brain tissue along white matter tracts and blood vessels [5, 6]. However, it has yet to be elucidated whether this biological phenomenon is due to the biochemical or biomechanical cues provided by these structures. It is critical to understand why these tumor cells migrate along these nanotopographical paths in order to develop therapies to inhibit the migration of these tumor cells from the primary tumor mass.

Cellular biomechanics are responsible for a variety of biological functions in eukaryotic cells, including migration, differentiation, morphogenesis, and proliferation [7, 8]. Specifically, these processes are largely dependent on the cytoskeleton structure and its response to the surrounding extracellular matrix (ECM). Cells adhere to the local substratum via integrins, which cluster together leading to the recruitment of proteins necessary for the formation of focal adhesions and stress fibers [9]. Topographic organization of the ECM plays a key role in directing cell behavior by providing three-dimensional cues to the cell [10].

The cytoskeleton and ECM are drastically altered in brain tumors. The actin filaments of cancer cells are transformed and their adhesion to the surrounding ECM is modified. Upon oncogenic transformation, the actin cytoskeleton is reorganized to allow for an elongated cell morphology aiding in directional migration [11]. Further, actin-rich membrane protrusions, including, including lamellipodia, filopodia, and invadopodia, are formed along the leading edge of the cell and release proteinases to degrade the surrounding ECM, further aiding in cell migration [11-13]. Together, this affects the cells'

deformation, altering their ability to stretch and contract. As these cells are more deformable, it is much easier for these cells to invade through tighter spaces compared to a healthy cell that is less deformable [12]. The cytoskeletal stiffness of cells has been shown to correlate with the migratory and invasive potential in a variety of cancer types, including ovarian, breast, prostate, and bladder, but has yet to be investigated in GBM [14-20].

It is difficult to understand the invasive nature of these cells without a comparable *in vitro* model that is able to recapitulate the complex *in vivo* tumor microenvironment. While the ideal approach would be to use an *in vivo* tumor model, limitations with current technology do not allow for monitoring at the microscopic, single cell level. In addition, traditional *in vitro* models employed to quantify migration use rigid 2D substrates, which do not provide a true assessment of tumor invasion due to their lack of nanotopography and appropriate substrate stiffness. By developing an *in vitro* model that mimics the *in vivo* microenvironment, systematic studies may be completed to better evaluate the molecular mechanisms responsible for tumor cell migration, as well as the cellular responses to the nanotopographic cues. Jain *et al.* previously fabricated a thin film made of aligned electrospun polymeric nanofibers that mimicked the nanotopographical cues provided by the white matter tracts and blood vessels, and showed that intracortical tumor cells on the film were predominantly in a migratory state than proliferative state. Cells on the aligned fibers migrated much further than those on a substrate without topography [21]. In addition to modeling GBM migration, electrospun nanofibers have also been used as a model for breast cancer cell invasion [22] and embryonic myogenesis [23].

In this study, we investigated the mechanical differences between healthy cells and GBM tumor cells, as well as how the alignment and nanotopography of the nanofibers affect the tumor cell response in terms of their migration/invasion potential. As seen in other cancer types, the more invasive, malignant tumor cells were softer than less invasive tumor cells and their respective healthy, non-mutated cells [16, 18, 20, 24]. To our knowledge, investigating the invasive potential in relation to cytoskeletal stiffness for GBM tumor cells has not been previously reported. In addition, by using an aligned nanofiber film to mimic the white matter tracts and blood vessels, we demonstrated that nanotopography affected cellular biomechanics. By examining the cytoskeletal stiffness, cytoskeletal organization,

and gene expression of GBM cells cultured on aligned nanofibers, randomly aligned nanofibers, smooth film, and tissue culture polystyrene (TCPS), we identified substrate nanotopography is correlative with the GBM tumor cells' propensity to be in a more migratory or proliferative state.

CHAPTER 2: REVIEW OF LITERATURE

2.1. GLIOBLASTOMA MULTIFORME

Primary brain tumors are an abnormal mass of mutated cells that originate in the brain. Tumors that arise from glial or precursor cells are called gliomas, and account for about 80% of malignant primary brain and central nervous system (CNS) tumors. Gliomas are classified into four histological grades (I-IV, in increasing aggressiveness) based on their abnormality and growth rate. Glioblastoma multiforme (GBM, WHO grade IV) is a malignant brain cancer that is believed to arise from astrocytes. While it is rare, with an incidence rate of 3.19 per 100,000 person-years, it is the most common malignant primary CNS tumor, accounting for 45.6% of primary malignant brain tumors [1]. Current treatments include surgical resection, chemotherapy, and radiotherapy, however even with these treatments; average survival time is about 14.6 months [2]. Furthermore, even after the tumor is removed, recurrence is virtually inevitable (~90% recurrence rate) due to the extensive invasive nature of GBM cells [3].

While it is uncommon for GBM cells to metastasize to other areas of the body, one of the hallmarks of this disease is that individual tumor cells have the ability to diffusely invade healthy brain tissue. This makes complete removal of the tumor difficult, despite multi-modal treatments. Tumor cells can cross hemisphere, and have been shown to migrate more than 4-7 cm from primary tumor sites, leading to secondary tumor sites [25]. As shown in Figure 1, the main means of migration is along white matter tracts and blood vessels of the brain, which act as 'highways' for cell migration [5, 6]. Cellular mechanisms responsible for the migratory nature of these cells remain a research focus.

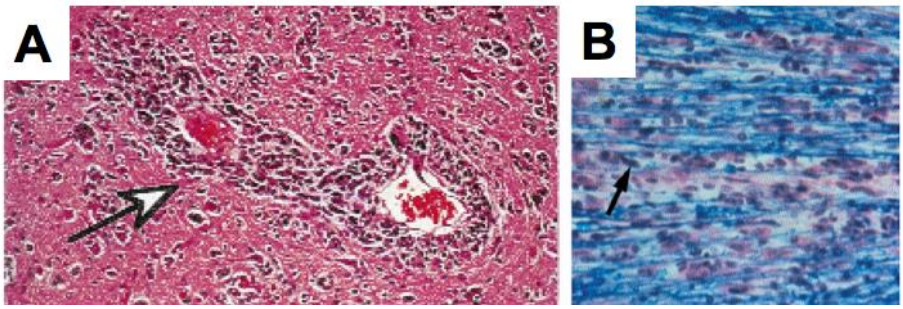

Figure 1: GBM tumor cells migrating along blood vessels and white matter tracts. A) Histologic section of GBM cells surrounding vessels (arrow) [6]. B) Histologic section of corpus callosum, myelinated axons stained blue. Arrow indicates migrating cell [5].

The cancer initiating cells (CICs, also called cancer stem cells), a subset of the heterogenic cell population, are highly migratory, invasive, resistant to therapy, and responsible for the recurrence of the tumor [4]. These cells are characterized as their ability to self-renew, aberrantly differentiate, initiate tumorigenesis, and migrate [26]. While established human glioblastoma cell lines, such as U87MG and A172, have been used to model GBM and in drug treatment assays, the phenotypic characteristics and genetic modifications bear little similarity to cells isolated from the heterogenic primary brain tumor. Therefore, the use of GBM models based on CICs, specifically primary CICs, is more biologically relevant and has implications for the better understanding of tumor biology and development of new therapies [27].

2.2. CELLULAR BIOMECHANICS/CYTOSKELETAL DYNAMICS AND BIOMECHANICS

Cell mechanics are responsible for a variety of biological functions in eukaryotic cells, including migration, differentiation, mechanotransduction, morphogenesis, and proliferation [7, 8]. Specifically, these processes are largely dependent on the cytoskeleton and its interactions with the surrounding ECM. The cytoskeleton is the cell's internal scaffolding, which is comprised of an interconnected network of biopolymers and proteins. Collectively, the cytoskeleton organizes contents of the cell, connects cell both with the surrounding ECM, and aids in generating force that facilitates cell motility [28]. The architecture and organization of the different cytoskeleton components alter the shape and mechanical response within the cell, which in turn, affects the cell-cell and cell-matrix interactions. These changes can alter the mechanical properties in cells, and can lead to disease development [9, 28].

The cytoskeleton of eukaryotic cells contains three distinct polymeric structures: actin microfilaments, intermediate filaments, and microtubules. Actin exists as a free monomer G-actin (globular) or as a linear polymer F-actin (filamentous), both of which are important for cell motility and contraction. F-actin can further be organized into stress fibers, or closely packed arrays of filaments, and are formed when the cell needs additional strength, such as during migration. F-actin filaments also concentrate around focal adhesion sites. Similar to actin, intermediate filaments aid in the maintenance of cell shape and provide structural integrity for the cell. Named intermediate due to their approximate diameter of 10 nm, their size is in-between the diameter of actin microfilaments (7 nm) and microtubules (25 nm). Finally, microtubules consist of alpha-tubulin and beta-tubulin, which dimerize to form a long, hollow, tubular structure. Microtubules aid in dictating cell shape, and play a role in cell migration and mitosis [29, 30].

Cells are able to sense their external environment and create signals through adhesions onto the substratum Adhesions of the cells to the ECM are predominantly modulated via integrins. Integrins are transmembrane receptors that give cells a connection to the ECM, and communicate signals from the cell to the surrounding space. In cell invasion, integrins recruit proteases to the leading edge of the cell, which aid in breaking down the surrounding matrix [31]. When cells attach to the ECM, integrins cluster on the cytoplasmic portion of the cell surface, and are bound together by crosslinkers that bind the cytoplasmic tails of the integrins together [32]. Clustering leads to the recruitment of adaptor/scaffold and signaling proteins, including talin and vinculin, that form focal adhesions, which link the actin cytoskeleton firmly to the ECM. Talin initiates focal adhesion assembly by linking the cytoplasmic portions of the integrins to either actin binding proteins α-actinin and/or vinculin [9].

Focal adhesion presence plays a role in cell morphology, as formation of focal adhesions leads to cells with spread morphology. Without focal adhesions, there is reduced substrate adhesion, and an increased population of non-adherent cells. Focal adhesion formation also plays a role in cell motility, as when focal adhesions grasp the surrounding ECM along the leading edge. The traction forces within the cell are generated, which are necessary to move the cell forward. In order for the cells to migrate, however, the cells

must also release from the ECM. By synchronizing a formation and turnover of focal adhesion attachment at the leading edge and trailing edge, respectively, cells will migrate forward (Figure 2). Thus the generation and turnover of focal adhesions along the leading and trailing edge, respectively, is vital for the continuous directional migration of cells [9].

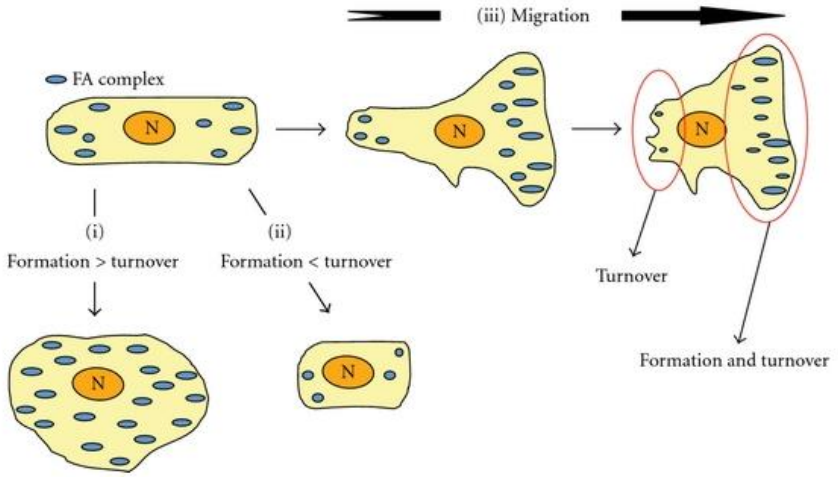

Figure 2: Focal adhesion formation during cellular migration. An imbalance of formation and turnover of focal adhesions within the cell to the ECM leads to either a stable adhesion (i) or unstable adhesion (ii). Rapid formation and turnover at the leading edge of the cell, along with turnover of focal adhesions at the trailing edge, leads to promoted migration (iii) [9].

Different processes regulate the assembly/disassembly of focal adhesions. For example, Rho/ROCK is one pathway that regulates the clustering of integrins on the cell surface. When microtubules extend to the focal adhesions, the integrins disassemble and internalize from the surface [9]. In addition, adaptor protein, paxillin, binds to vinculin, and provides a platform for protein tyrosine kinases, such as focal adhesion kinase (FAK) [33]. FAK is responsible in the turnover of focal adhesions, which is necessary to allow cell migration. Overexpression of FAK has been correlated with enhanced migration and increased invasive potential in human tumors [34, 35].

Substrate and ECM nanotopography also have an effect on stress fiber and focal adhesion formation. Human mesenchymal stem cells cultured on 350 nm gratings of TCPS exhibited increased expression of integrin subunits compared to unpatterned controls. In addition, the cells on the nanotopographic substrates exhibited an elongated morphology with an aligned actin cytoskeleton and a dense focal adhesion population around the poles

of the cells, compared to a random dense network on the unpatterned control [10]. Similar results were found across a variety of cell types including epithelial, kidney, and fibroblast cells [36-38].

2.2.1. Cell Mechanics and Disease

Cellular behavior, as well as the cytoskeleton, is altered in a disease state. Due to technical advancements, cellular mechanics has been a research focus to identify relationships between cell structure, biomechanics, and disease states [12]. Cells are dynamic and are continuously changing and responding to their chemical and mechanical environment. In order to identify a relationship between the chemobiomechanical pathway and disease, systematic studies must be completed under conditions that mimic the *in vivo* microenvironment. The lack of a comparable model limits the amount of comprehensive studies completed.

The cytoskeleton and ECM are drastically altered in cancer. The actin filaments of cancer cells are transformed, ultimately affecting their deformation. This transformation alters cellular ability to stretch and contract, which allows cells to migrate through tissues much faster and easier than normal cells, leading to tumor metastasis [12].

2.2.2. Mechanics and Biology of Glioblastoma

Cellular migration is an important process that is facilitated by several mechanical processes including adhesion and force generation within the cell. Thus, it is important to understand the molecular mechanisms behind the migration of glioblastoma cells in order to develop therapies to inhibit the outward growth of cells from the primary tumor mass. It has been previously determined that glioblastoma cells preferentially invade along the blood vessels and white matter tracts in the brain. Unlike in other cancer types, GBM tumors do not invade into blood vessels, and rarely metastasize to other organs. This is believed to be due to the specialized brain ECM compared to other organs. In addition to being softer than other tissue, brain ECM has a low percentage of fibrous proteins such as collagen and laminin, and is instead largely comprised of hyaluronic acid (HA), a non-sulfated glycosaminoglycan. HA is believed to play an important role in GBM progression, as malignant gliomas have exhibited greater concentrations of HA than normal brains [39].

Cell invasion is dependent on tumor cell attachment to the ECM via cell surface markers and integrins. The signal transduction from HA causing the cells to migrate is partly due to the cell-surface receptor CD44, which is correlated with malignancy in gliomas. CD44 activation promotes downstream signaling of Rho family GTPases, ultimately leading to migration. Degradation of ECM by hydrolytic enzymes secreted by the tumor cells creates the intracellular space for tumor cells to migrate into. The actin cytoskeleton rearranges and is extended into the newly remodeled ECM, leading to focal adhesion formation at the leading edge, generating the traction necessary to move the cell forward [40].

There are many molecular pathways that have been implicated in glioblastoma migration, including the Notch pathway. This pathway is important for embryonic development, however, has also been implicated in cancer progression. Notch exists as 4 highly homologous large transmembrane receptors (1-4) consisting of an extracellular, transmembrane, and an intracellular domain (NICD). When either of the Notch receptors is activated, NICD is cleaved and released from the membrane, which translocates to the nucleus leading to transcription of downstream target genes [41].

Notch deregulation is also believed to play a role in epithelial-mesenchymal transition (EMT), which plays a role in tumor aggressiveness and progression. EMT is a process in which epithelial cells undergo morphological changes characterized from the epithelial phenotype, with high expression of E-cadherin, actin cytoskeleton organization, and tight cell-cell contacts, to the elongated mesenchymal phenotype, with increased N-cadherin expression and cell-matrix interactions. Similar to the Notch pathway, EMT is linked with embryogenesis as well as tumor progression and metastasis. Specifically, translocation of E-cadherin from the cell membrane to the nucleus leads to induction of EMT. Repression of E-cadherin via the transcription factors SNAI1, TWIST, and ZEB1 aid in driving cancer development [42]. Notch has been shown to promote EMT through the regulation of SNAI1. Zhang *et al.* showed that elevation of Notch1 signaling in GBM cells and in tumor biopsies led to increased tumor metastasis and EMT markers [41]. The authors proposed that Notch signaling resulted in AKT activation, which in turn resulted in increased NF-κB and β-catenin signaling. Together, this increased signaling resulted in the

promotion of cell migration and invasion by the upregulation of EMT markers SNAI1, ZEB1, and vimentin [41]. Notch is believed to affect SNAI1 through by recruiting the NICD to the Snai1 promoter [43].

As discussed earlier, in order for cells to invade surrounding tissue, they must degrade the surrounding matrix. The proteolytic enzymes responsible for this degradation include matrix metalloproteinase-2 (MMP-2) and MMP-9, which have been closely correlated with glioblastoma invasiveness [44, 45]. The metastasis suppressor gene reversion-inducing-cysteine-rich protein with kazal motifs (RECK) negatively regulates MMP-2 and MMP-9 by directly inhibiting membrane protease activity, influencing their release from the cells, and sequestering of MMPs at the cell membrane [46]. Downregulation of RECK is essential for the invasiveness of GBM cells [47]. Silveira Corrêa *et al*. has shown the effect of RECK expression on the cytoskeleton of the T98G glioblastoma cells. Cells transfected to overexpress RECK were closely packed together and exhibited few lamellipodia and greater amounts of stress fibers, indicating decreased cell motility. The control cells however were more polarized in the direction of migration, and had the presence of lamellipodia and stress fiber formation [48].

Cyclin dependent kinases (CDKs) and cyclins are a research focus for GBMs as regulators of cell cycle progression. CDK20 (also called cell cycle-related kinase) is a CDK-activating kinase that is important for the cell cycle [49]. Elevated levels of CDK20 have been reported to be essential for proliferation in a variety of cancer cell lines, and is believed to play an oncogenic role in GBM. CDK20 suppression arrests cells at the G0-G1 phase by decreasing CDK2 phosphorylation, and also knockdowns expression of cyclins in human cancers, including glioblastoma [49-51]. Specifically, CDK20 expression is correlated with cyclin D1 expression, which is required for progression through the G1 phase [49, 52].

In addition, there is an observed dichotomy between proliferation and migration in GBMs, also known as the “go-or-grow” phenomenon. With GBM cells grown *in vitro*, the invasive tumor cells along the leading edge exhibited a decreased proliferation rate compared with the tumor core. Similarly, when cells were grown on a permissive ECM that

supported migration, cells exhibited a more migratory phenotype instead of a proliferative one, compared to the non-permissive substrate which exhibited the opposite [53]. Similarly, soluble mitogens, such as transforming growth factor beta 1 (TGF-β1), have been shown to stimulate tumor invasion and suppress proliferation *in vitro* [54]. Cells transfected to express receptor tyrosine kinase EphB2 to promote migration exhibited a reduced cyclin B and cyclin D1 expression, indicating reduced proliferation [55]. Furthermore, with cells that were selected for an enhanced migratory phenotype, the growth rate was slightly impeded compared with the normal cell population [56].

Similar results have also been observed *in vivo*. Using stereotactic glioma biopsies, invasive cells in the white matter and cortex exhibited a decreased proliferative index. Similar results were also observed with invading cells that were far from the tumor core [57]. Using an implantable nanofiber film to direct tumor cell migration, Jain *et al.* showed that cells were in a less proliferative state on the aligned fibers compared to a smooth film control, as indicated by a reduced Ki-67+ staining. As shown in Figure 3, F-actin staining analysis showed that cells grown on the aligned film exhibited fibrous F-actin staining versus more punctate F-actin on smooth film, suggesting a more suspended state on the smooth film [21].

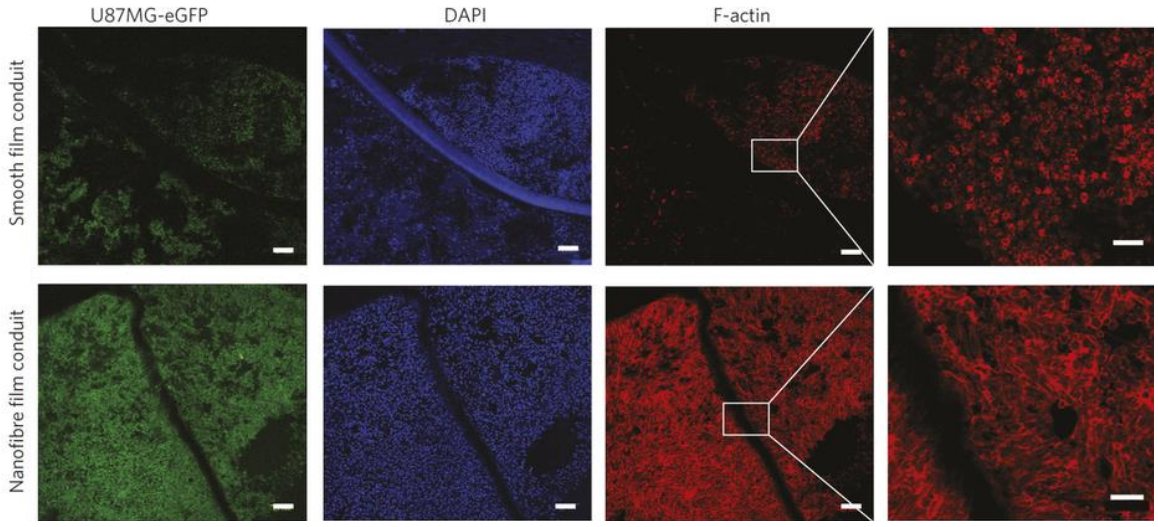

Figure 3: GBM cells on aligned fibers exhibit migratory phenotype. Actin (red) of cells on smooth film exhibited punctate filaments indicating a suspended, less migratory state. Uniform actin filaments were exhibited on tumor cells on aligned nanofiber film. Scale bar = 400 μm [21].

2.3. Assessing the Mechanical Properties of Cells

As mentioned earlier, cellular mechanics are currently being researched to identify biophysical markers for diseases. Cytoskeletal stiffness and traction forces are two biophysical properties that have been investigated in other cancers, but have yet to be fully investigated in glioblastoma. These two properties can be assessed via atomic force microscopy (AFM) and traction force microscopy (TFM), respectively.

2.3.1. Cytoskeletal Stiffness

Cells are considered a viscoelastic material as they display both elastic and time-dependent responses to deformation [58]. Recently, there has been increasing evidence that mechanical changes, specifically the cytoskeletal stiffness, at the single cell level are correlative with human disease, including cancer. Several biophysical adaptations are often associated with cancer cells as they become more invasive or metastatic. As previously mentioned, these cells often express fewer adhesion receptors, leading to more rounded cell morphology as well as a loss of cytoskeletal tension. Cell tension in healthy cells is a factor in cytoskeletal properties including stability, remodeling, stiffness, and traction, the latter two being important in this study [59]. Thus, researchers have been studying how cancer progression may be linked with cytoskeletal mechanics.

Several methods have been developed to determine cell stiffness, including using optical tweezers or an atomic force microscope (AFM) [58]. AFM is a surface characterization technique that has also been adopted for imaging and characterization of biological samples due to its high sensitivity and spatial resolution. In its simplest form, the AFM consists of microscopic-sized tip connected to a cantilever beam, which is used to indent/interact with the sample. The tip of the cantilever can come in a variety of shapes and sizes depending on its application. As shown in Figure 4, the tip is the part of the probe that comes in contact with the cell, while the cantilever itself acts as a spring to measure the contact force. A piezoelectric actuator is used to move the AFM probe in the Z-direction toward or away from the material. The shape and material of the cantilever probe are used to calculate its spring constant, and together with laser tracking of the cantilever deflection

to a photodetector, contact force can be calculated. Cell elasticity can then be calculated by calculating the force versus indentation data [58-61].

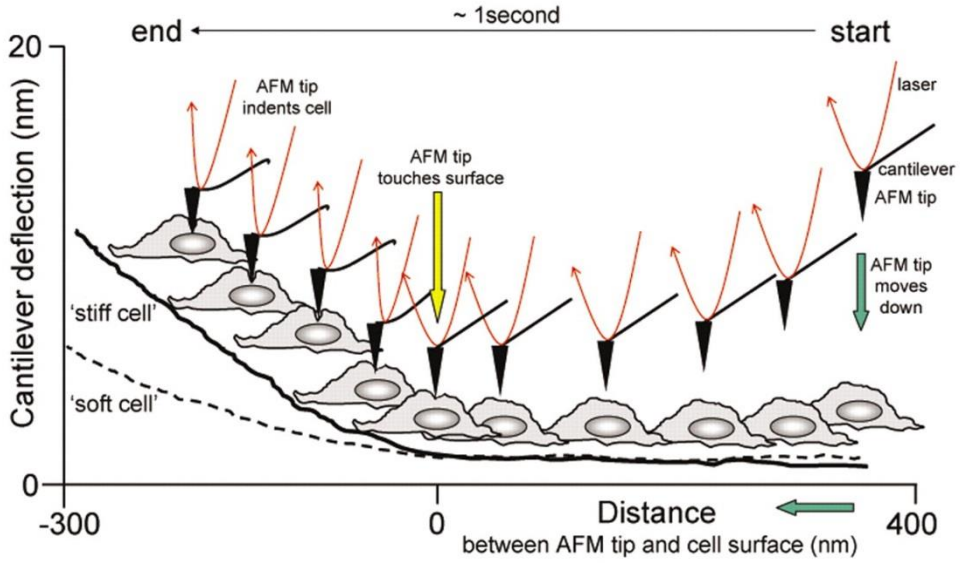

Figure 4: Outline of how cell stiffness measurements are performed on living cells using AFM. From right to left, as the AFM tip approaches the cell and makes contact with it, the cantilever bends, altering the laser beam deflection angle. A stiffer cell will result in a steeper deflection curve than a soft cell [62].

AFM is a useful tool for probing cellular mechanics. By using this technique, it has been reported that actin filaments are highly important in the mechanical stability of living cells, while microtubules do not have any effect on elasticity [63]. In addition, it has also been reported that the actin cytoskeleton/organization plays a role in human mesenchymal cell mechanical properties during differentiation [64]. In 2003, a link between AFM mechanical measurements and detection of disease was first suggested [61]. Moving forward, it was then shown that the cytoskeletal stiffness of breast [16], ovarian [18], prostate [24], lung, and pancreatic cancer cells [20] were intrinsically softer than their normal/healthy counterparts. In an ovarian cancer study, highly invasive cancer cells were less stiff than their less invasive parental cells, further suggesting the cytoskeletal stiffness can be used as a biomarker for invasive potential [18]. To our knowledge, a comparative study of the cytoskeletal stiffness of non-malignant astrocytes, GBM cell lines, and primary GBM CICs has yet to be reported.

2.3.2. Cell Traction Forces

When cells attach to a substrate, they spread and generate intracellular traction forces through ATP-fueled actomyosin interactions [65]. Cell traction forces play a role in migration, as these forces need to be generated and exerted to the ECM or substratum to move the cell forward. In addition, during cell migration, actin polymerization and focal adhesion assembly at the leading edge of the cell also produces traction forces. The turnover of focal adhesions at the leading and trailing edge aid in the directional cell migration [65, 66].

Traction force microscopy (TFM) is a technique used to quantify cellular traction forces and stresses. While a variety of TFM techniques exist, the basic principle is to determine the displacement of the stressed ECM or substratum at the surface of the cell to create a stress vector. The strain and elastic modulus of the substrate can then used to calculate the traction forces. While some methods involve culturing cells on pillars [67] or within 3D hydrogels [68], in this study, cells were grown on a flexible polyacrylamide gel with fluorescent microbeads to aid in determining substrate displacement.

It has been shown previously that metastatic breast, prostate, and cancer cell lines exert more traction forces than their non-metastatic counterparts [69]. Conversely, an in-depth study of comparing the traction forces in breast cancer cells with varying degrees of metastatic potential showed that the more invasive cells produced less traction force than the control cells and less invasive counterparts [70]. Thus, as the relationship between traction force and invasiveness varies between different types of tumors, more investigation of traction forces and cancer cell migration in GBM needs to be completed to help explain this phenomenon.

2.4. IN VITRO MODELS

2.4.1. TRADITIONAL MODELS

In order to identify the relationship between the biomechanical pathway of cells and disease, systematic studies must be completed under conditions that best mimic the *in vivo* microenvironment. The easiest, and most commonly used, model to quantify migration is the scratch test/wound-healing assay. With this test, cells are grown as a monolayer on tissue culture plastic, and a 'scratch' is made using a pipette tip to mimic a wound. Cells

migrate into this space and close the wound, which is then used to determine the migration rate of the cells. While this test is easy to conduct and requires minimal resources, the lack of topography and the use of a rigid plastic substrate that is not comparable to a living tissue does not provide a true assessment of cell migration or invasion.

Second, polyacrylamide gels have also been researched as a model. The mechanical properties of the gels are highly tunable and can highly resemble the stiffness of the brain ECM. Groups have also been used three-dimensional hyaluronic acid gels to better resemble the brain ECM composition and model cell infiltrative behavior [39]. While these gels can mimic the stiffness and matrix of the tumor environment, they do not mimic the topography that these tumor cells migrate along, and thus do not meet the needs of this study.

Organotypic brain slices have also been used to quantify cell migration. Brains are isolated from an animal model, and cut into 300 μm thick slices. Cells are then seeded in the area of choice on the slice, and outgrowth and migration from the region is measured [71]. While this model has the benefit of having a similar ECM and nanotopography of the native brain, the high cost of animal studies and large sample-to-sample variation between brains make them difficult to work with. In addition, the lack of stability in the slices hinders them from being used for long-term studies.

Thus, *in vitro* assays that more closely mimic the *in vivo* microenvironment need to be developed as they can better assess and characterize cancer cell migration and its abnormal proliferative capabilities, leading to the development of anti-invasive drugs, ultimately providing patients with better and more effective therapies.

2.4.2. ELECTROSPINNING

In order to create a scaffold that mimics the nanotopography of the white matter tracts and blood vessels, a nanotopgraphic film with submicron diameters needs to be developed. Fortunately, electrospinning is a process that can be used to meet this need. Originally discovered in 1934 when an electric field was used to produce polymer threads, electrospinning is a material fabrication technique that creates long, continuous nanofibers through an electrically charged jet of polymer solution. In its basic form, a polymer solution

is infused through a syringe and is charged with a high voltage (Figure 5). A droplet from the charged polymer is elongated into a conical shape (Taylor cone), and a thin fiber is ejected from the droplet, which accumulates onto a grounded collector [72, 73].

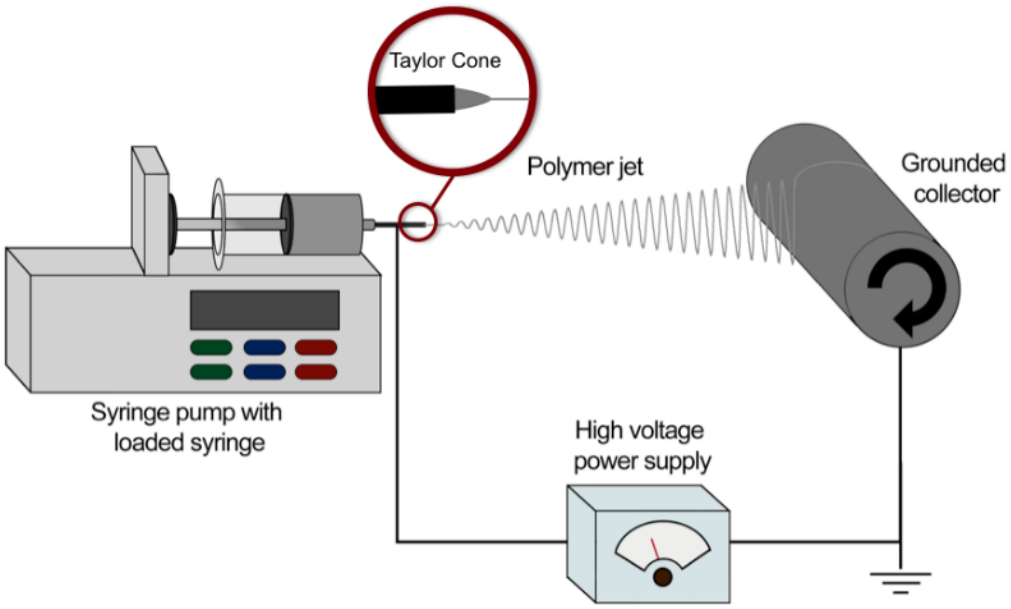

Figure 5: Schematic of electrospinning apparatus. Using a rotating mandrel as a grounded collector, aligned nanofibers will be generated.

The process is highly tunable, as the controllable parameters such as electric field between the nozzle and collector, flow rate, deposition distance, and polymer concentration all play a factor in the fiber properties. For example, the deposition distance affects how much solvent is evaporated, thus the greater the distance, the thinner the fibers. In addition, the orientation of the fibers can change based on the collector. When fibers accumulate on a static collector, randomly oriented nanofibers are created. However, when a rapidly rotating mandrel is used, highly aligned nanofibers can be generated [73].

Electrospinning can be used in a variety of applications in the biomedical field, including drug release, wound dressing, and tissue engineering. Due to its highly tunable properties and nano-scale, electrospun nanofibers can mimic the properties of the ECM to allow researchers to examine cell behavior *in vitro* in a physiologically relevant environment [73]. Electrospun nanofibers have been used to investigate the relationship with topography on the osteogenic differentiation of bone marrow stromal cells [74],

neurite outgrowth from dorsal root ganglia [75], and myogenic differentiation from embryonic stem cells [23].

More important for matters of this study, electrospun nanofibers have been investigated as mimetic model for cancer cell invasion, specifically in breast cancer and GBM. The nanofibers mimic the tumor-associated collagen signatures associated with metastatic breast cancer [50]. In addition, Jain *et al.* previously demonstrated that an aligned nanofiber model closely resembles the nanotopography of the white matter tracts and blood vessels that the tumor cells migrate along in GBM [21]. Aligned nanofibers have been shown to lead to significant increases in migratory related genes and proteins [76, 77]. In addition, GBM tumor cells on aligned nanofibers were significantly faster and migrated further than when cultured on random nanofibers [76, 78]. Specifically, Johnson *et al*. found that effective velocities of GBM cells on the aligned fibers were 4.2 ± 0.39 μm/hr on aligned nanofibers, compared to 0.8 ± 0.08 μm/hr on the randomly oriented nanofibers [77]. Jain *et al*. also observed similar trend in GBM cell speed, with cells on aligned fibers migrating up to 3-fold faster than those migrating on a smooth film control [21]. By using this nanofiber model to mimic GBM cell migration, relationships between the biomechanical pathway and this disease can be systematically investigated and elucidate the enhanced migratory mechanism involved in this disease.

CHAPTER 3: HYPOTHESIS AND SPECIFIC AIMS

As it is difficult to understand the mechanism of GBM migration using an *in vivo* model due to limitations with current technology, *in vitro* models that closely mimic the tumor microenvironment are increasingly alluring. By using smooth film, random nanofibers, and aligned nanofibers that mimic the nanotopography, specifically the alignment and nanofiber diameter, of the tumor microenvironment, systematic studies can be completed that can quickly identify the changes in GBM cellular mechanics. As it has been shown in other cancers that cell stiffness is correlative with more migratory cells, and that an aligned nanotopography promotes more motile GBM cells, *we hypothesized that aligned nanofibers induce mechanical changes within GBM cells (i.e. cytoskeletal stiffness) that enhance a migratory state*.

Specific Aim 1 – Determine baseline mechanical properties (i.e. cytoskeletal stiffness, traction force) of glioblastoma multiforme cells and identify if differences correlate with degree of malignancy.

We hypothesized that the more malignant cells will have stiffness due to their higher invasive potential. When a normal cell mutates and becomes tumorigenic, it develops invasive properties, which incorporate biomechanical changes. Rat pup astrocytes, human glioblastoma (GBM) cell lines, and primary human glioblastoma CICs were used to study the cell cytoskeleton and its properties using atomic force microscopy, traction force microscopy, immunocytochemistry for cytoskeleton staining.

Specific Aim 2 – Determine whether aligned nanotopography substrates enhance the migratory state in GBM cells.

We hypothesized that an aligned nanotopography substrate will promote a migratory cell state, as the aligned nanofibers mimic the paths tumor cells migrate *in vivo*. Nanotopographic substrates, aligned and randomly aligned nanofibers, and lack of nanotopography substrates, smooth film and tissue culture polystyrene, were used. Tumor cells were cultured on the different substrates, and cytoskeletal stiffness measurements were collected using AFM. Gene expression and cell cycle population were quantified using qRT-PCR and FACS to assess a relationship

between nanotopography and cell state. Further, vinculin and actin staining were used to identify cytoskeletal organization and assess a relationship between focal adhesions and an enhanced migratory state.

CHAPTER 4: MATERIALS AND METHODS

4.1. CELL CULTURE

Human glioblastoma multiforme tumor cell lines, U87MG and A172 (ATCC, Manassas, VA), were maintained and cultured in DMEM (Corning, Corning, NY), supplemented with 10% fetal bovine serum (FBS, Gemini Bio-Products, West Sacramento, CA), 1% penicillin-streptomycin, 1% L-glutamine, and 1% non-essential amino acids (Corning). U87MG cells expressing enhanced green fluorescent protein (eGFP) were generously donated by Dr. Ravi Bellamkonda (Georgia Institute of Technology). A172 cells were transfected using GFP-Actin fusion lentiviral particles (GenTarget Inc., San Diego, CA) and positive colonies were selected for expansion. Primary CICs, BT145 were generously gifted by Dr. Rosalind Segal (Dana-Farber Cancer Institute). The GBM CICs were cultured in DMEM/F12 (Corning), supplemented with B27 (Gibco, Life Technologies Grand Island, NY), 15 mM HEPES (Alfa Aesar, Ward Hill, MA), 20 ng/mL EGF (Invitrogen, Carlsbad, CA), and 20 ng/mL FGF (Invitrogen). Differentiated BT145 tumor cells were grown in DMEM supplemented with 10% FBS. Primary rat astrocytes were isolated from Neonatal Sprague-Dawley pups (post-natal day 2) and maintained in Neurobasal Medium (Gibco), supplemented with 10% FBS and 1X GlutaMAX (Gibco).

4.2. PREPARATION OF NANOTOPOGRAPHIC SCAFFOLDS

Aligned and randomly aligned nanofibers were fabricated using electrospinning as previously described [79]. Electrospinning was used to generate nanofiber films. Briefly, a 10% polycaprolactone (PCL, Sigma, St. Louis, MO) was made by dissolving PCL in 1,1,1,3,3,3-hexafluoro-2-propanol (HFIP, Sigma) overnight. Approximately 0.5 mL of polymer was loaded into a 5-mL plastic syringe fitted with a 19 gauge blunt tipped needle and placed 10 cm from the collector, an aluminum foil coated mandrel (2”D x 4”L). A positive voltage was applied to the polymer by connecting a lead from a high power voltage source to the syringe needle. To fabricate aligned nanofibers with a diameter of 600-800 nm, the syringe pump was set to flow rate 0.15 mL/hr, and charged with 5-8 kV (Figure 6). Fibers were collected for 20 minutes onto the mandrel spinning at 3000 RPM. To fabricate randomly oriented fibers, the flow rate was adjusted to 0.5 mL/hr, charged with 8 kV, and

collected for 10 minutes onto the mandrel spinning with at 15 RPM. To fabricate smooth film, 12% PCL was pipetted and spread onto a glass coverslip and the HFIP was evaporated under vacuum. Smooth film and TCPS were used as non-topographic controls.

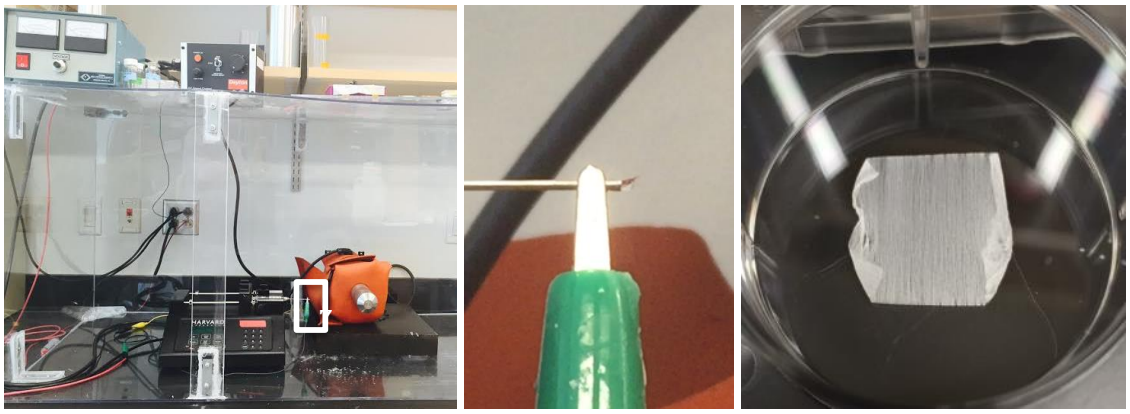

Figure 6: Electrospinning apparatus used in the Jain laboratory. Apparatus was maintained in a plastic enclosure for safety as well as to minimize any environmental factors. White box highlights tip of syringe (middle panel). When sufficient voltage is applied, droplet is elongated and Taylor cone is formed. After fiber spinning is complete, they are isolated and placed into tissue culture dishes where they are prepared for culturing (right panel).

Following preparation, substrates were dried overnight to allow for residual solvent to evaporate. Samples were cut to fit into 60 mm dishes, and submerged in 100% ethanol, and removed from the glass/foil. After the ethanol evaporated, substrates were secured to petri dishes using UV glue. Prior to use, substrates were sterilized under a UV lamp for 30 minutes, and coated with PureCol® Bovine Collagen (100 µg/mL, Advanced BioMatrix, San Diego, CA) for 1-2 hours at and allowed to incubate at 37°C to facilitate cell attachment. The substrates were then washed 3 times with sterile phosphate buffered saline (PBS) prior to seeding the cells.

4.3. Characterization of Substrates

To characterize the substrates, SEM was performed on the aligned nanofibers, randomly aligned nanofibers, and smooth film substrates as previously described [21]. Briefly, samples were mounted onto stubs using carbon tape. Smooth film SEM images were taken using a FEI-TeneoLoVac SEM and aligned and randomly aligned nanofiber films were taken using a JSM-7000F SEM. Fiber diameter and degree of alignment analysis was completed using ImageJ.

4.4. Cytoskeletal Stiffness Measurements

To measure the cytoskeletal stiffness measurements, tumor cells were seeded on the collagen-coated tissue culture polystyrene (TCPS) or PCL substrates at a density of 20,000 cells per sample (Figure 7). The tumor cells were cultured for 24 hrs prior to testing. An MPF3D-Bio AFM (Asylum Research, Santa Barbara, CA) was used to measure the stiffness of cells as previous described [80]. Briefly, the DNP-D cantilevers were calibrated using the thermal method prior to experiment. A Nikon Ti-S microscope (MVI, Avon, MA), was used to observe and select the desired cells for measurement. The AFM cantilever was placed over the perinuclear region of the cell, and an indentation was performed with a maximum cantilever deflection of 10 nm. After maximum deflection, the z-position of the AFM scanner was oscillated with a frequency of 10 Hz, amplitude of 25 nm, and duration of 1.5 seconds. The AFM tip was removed from the cell, and the z-position of the tip and cantilever deflection was recorded. A total of 3 measurements were obtained at different locations in the perinuclear region of the cell, a minimum of 15 cells was measured for each sample, and each sample was tested in biological triplicates. The Hertz indentation model was used to calculate the stiffness of each cell using a custom MATLAB (MathWorks, Natick, MA) code.

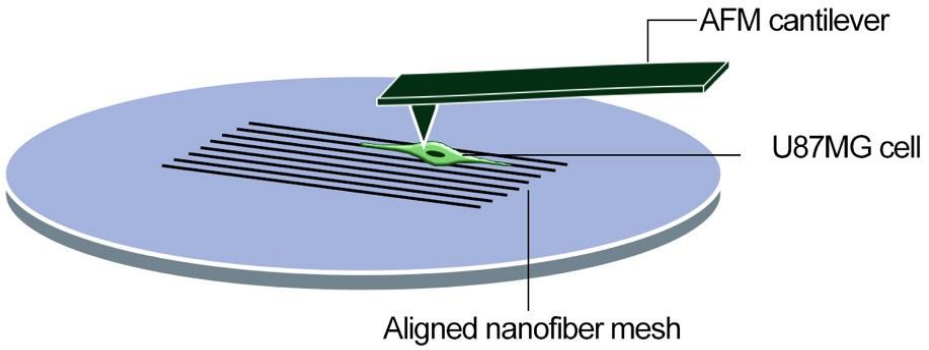

Figure 7: Schematic of how AFM was conducted on tumor cells on nanofiber substrates.

4.5. Cell Traction Forces

Traction force measurements were determined by culturing cancer cells on polyacrylamide gels with a thin layer of fluorescent beads embedded within them. Briefly, 2% 0.2-micrometer diameter FluoSpheres (Life Technologies) were diluted 1:200 in

ethanol, and 50 µl was pipetted onto clean, plasma treated 25x25 mm glass slides and placed in a 150 ^{o}C oven to facilitate an even distribution of spheres across the glass. Next, polyacrylamide solutions of 5% or 8% acrylamide and 0.08% or 0.1% bis-acrylamide, respectively, were made. Following, 64 µl of gel were pipetted onto 25x25 mm glutaraldehyde treated glass slides, and the glass slide with beads was gently placed on top, with the bead-coated slide of glass being in contact with the gel. After 7 minutes, the slides were separated using a razor blade. Slides were subsequently glued into customized petri dishes using UV glue, and hydrated using HEPES buffer until ready for use.

Prior to plating, the gel was treated with sulfo-SANPAH (Pierce) and coated with PureCol® Bovine Collagen (100 µg/mL, Advanced BioMatrix, San Diego, CA). For sulfo-SANPAH linkage, 500 µL of HEPES, 4 µL DMSO, and 0.5 g of sulfo-SANPAH were mixed and 250 µL was pipetted onto each gel. Gels were placed under UV for 10 minutes to activate the crosslinker to bind to the gel. Gels were then rinsed with HEPES and coated with collagen, and incubated at 4^{o}C overnight. After coating, collagen was removed, and rinsed 3 times with HEPES. Once completed, 10,000 cells were plated onto the gels. After 24 hours, fluorescent images of the spheres and brightfield images of cell on the stressed gel were taken using an Olympus IX83 microscope. Healthy cells, isolated from other cells were chosen, as it minimized any confounding effects from other cells exerting forces on the gels. Following initial imaging, media was removed, the plate was washed once with PBS, and 0.25% trypsin EDTA (Corning) was added to release the cell from the substrate. After five minutes, cells detached from the substrate, and the gel returned to a relaxed state. Corresponding images of the beads were taken at the same location. Traction forces were calculated using MATLAB and ANSYS software (ANSYS Inc., Canonsburg, PA). A minimum of 7 cells were analyzed for each gel, and three gels were analyzed for each cell type.

4.6. Cytoskeletal Staining and Analysis

Approximately 15,000 tumor cells or astrocytes were cultured on collagen-coated substrates overnight (about 24 hours) before being briefly rinsed with cytoskeleton buffer. Following this, cells were fixed with 4% paraformaldehyde for 10 minutes, permeabilized with 0.1% Triton-X-100 (Sigma) for 20 minutes, and blocked in 4% goat serum for 30

minutes. Cells were then incubated at 4 ^{o}C overnight with primary antibody for focal adhesion protein vinculin (1:500 in 4% goat serum in PBS, Sigma), then rinsed three times with PBS. Secondary antibody, Alexa-Fluor 594 goat anti-mouse (1:220, Invitrogen) in 2% goat serum in PBS, was used and incubated at room temperature for two hours. Slides were rinsed again with PBS, and F-actin was stained using phalloidin (Life Technologies) for 30 minutes. Slides were rinsed again in PBS and counterstained with Hoechst 33342 (1:5000, Life Technologies) for 10 minutes. Coverslips were rinsed again, and glass slides were mounted using Fluoromount-G. A Leica SP5 Point Scanning Confocal microscope was used to visualize the cytoskeletal organization on the substrates. Due to the nanotopography on the nanofibers, Z-plane stacks and standard deviation z-projection were used to produce images on nanotopographic substrates.

ImageJ (NIH, Bethesda, MD) was used to analyze the amount of positive vinculin staining when cultured on glass. Quantification of the focal adhesions from the collected images was completed using a modified protocol by Hozrum, *et al*. [81]. Briefly, vinculin-channel images were imported into ImageJ, and the Subtract Background filter with a sliding paraboloid option with rolling ball radius of 50 pixels option selected. Next, local co-ntrast was enhanced using the CLAHE plugin, with parameters block size 19, histogram bins 256, maximum slope 6, no mask, and fast option selected. Next, mathematical exponential filter was applied to minimize background. Next, the brightness and contrast and threshold were automatically adjusted. Finally, the Analyze Particles command was executed and the amount of total positive staining was recorded, including staining localized in the interior region of the cell as well as the periphery of the cell. Next the total vinculin area was divided by the projected cell area. A minimum of 15 cells was imaged per substrate, and each substrate was imaged in triplicate.

In addition, morphometric analysis of the area, length, and shape factor ($4\pi(\text{area})/(\text{perimeter})^2$) of the focal adhesions of the cells were conducted on the collected images using ImageJ software. A minimum of 7 cells was analyzed for each substrate, and 3 substrates were analyzed for each condition. An average of each shape descriptor was calculated for each cell.

4.7. Analysis of Key Migratory and Proliferative Gene Markers

To analyze key migratory and proliferative gene makers, quantitative reverse transcription polymerase chain reaction (qRT-PCR) was performed. In order to collect the mRNA, 750,000 tumor cells were seeded onto each substrate. Twenty-four hours post-seeding, the media was removed and RLT Buffer (Qiagen, Venlo, Netherlands) was added to the cultures for 20 minutes to lyse cells. The solution was then collected, processed, and purified using the RNeasy kit (Qiagen). The mRNA concentration for each sample was measured at the 260/280 absorbance using NanoDrop 2000 spectrophotometer (Thermo Fisher Scientific). The cDNA was made using the equivalent of 1 μg of RNA and iScript cDNA synthesis kit (Bio-Rad, Hercules, CA). Migratory markers, zinc finger protein SNAI1 (SNAI1), Notch homolog 1 (NOTCH1), and reversion-inducing-cysteine-rich protein with kazal motifs (RECK), and proliferative markers, cyclin-dependent kinase 20 (CDK20), and cyclin D1 (CCND1), were probed using the iTaq SYBR Green Supermix (Bio-Rad). For analysis of each gene, and the values were normalized to the housekeeping gene GAPDH. Primer sequences are listed in Table 1.

Table 1: Forward and Reverse Primers

Gene	Forward Primer	Reverse Primer
GAPDH	5'-TGTAGTTGAGGTCAATGAAGGG-3'	5'-ACATCGCTCAGACACCATG-3'
STAT3	5'-CAGTGACCAGGCAGAAGATG-3	5'-GCTCACTCACGATGCTTCTC-3'
SNAI1	5'-GGTTCTTCTGCGCTACTGC-3'	5'-GCTGGAAGGTAAACTCTGGATT-3
NOTCH1	5'-CAGGCAATCCGAGGACTATG-3'	5'-CAGGCGTGTTGTTCTCACAG-3
RECK	5'-CAATAGCCAGTTCACAGCAG-3'	5'-CCAGATTATTGCCCAGAGACA-3'
CDK20	5'-CAGTGTCTGCCTTCTATCCTG-3'	5'-TGTACCACATACTGATTGTCCTC-3’
CCND1	5'-GCCCTCGGTGTCCTACTTC-3'	5'-CTGTTCCTCGCAGACCTCC-3'

4.8. FACS Cell Cycle Analysis

In order to synchronize populations into the G_0 phase, cells were serum started for 24 hours in 1% FBS. Upon subculture, 500,000 cells were plated onto collagen coated substrates in normal growth media. After 3 days, cells were trypsinized, fixed in 70% ethanol overnight and incubated with Ribonuclease A (Life Technologies) and propidium

iodide (Life Technologies) for 30 minutes. DNA content from single cells were analyzed using a BD Accuri C6 flow cytometer, and completed in triplicate.

4.9. Statistical Analysis

All statistical analysis was performed by using GraphPad Prism (GraphPad Software, San Diego, CA). Data were reported as mean ± standard error of the mean (SEM), and either a t-test or a one-way ANOVA with Tukey's post-hoc analysis was performed. Data were considered statistically significant with a p value < 0.05, unless stated otherwise stated.

CHAPTER 5: RESULTS AND DISCUSSION

In this study, we investigated how the cytoskeletal mechanical properties of GBM tumor cells correlate to their invasive potential. Additionally, we analyzed whether the cytoskeletal mechanical properties altered based upon the alignment and nanotopography of the substrates. Our data showed that the more invasive GBM tumor cells were more compliant and exerted less traction forces than the primary astrocytes that have less invasive potential. Furthermore, when seeded on an aligned nanotopographic substrate that mimicked the *in vivo* tumor microenvironment, cytoskeletal stiffness further decreased and an increased expression of migratory related genes were observed, suggesting that substrate nanotopography and alignment have an effect on the mechanisms involved in GBM invasion.

5.1. SPECIFIC AIM 1

5.1.1. GREATER CYTOSKELETAL STIFFNESS OBSERVED IN ASTROCYTES THAN IN GBM TUMOR CELLS

As GBM is categorized as a Grade IV astrocytoma, atomic force microscopy (AFM) was used to determine if there were differences in cytoskeletal stiffness between GBM tumor cells and non-cancerous, healthy primary astrocytes. For the GBM cells, GBM cell lines (U87MG and A172), and primary GBM CICs were used. Primary GBM most commonly arises directly from astrocytes or glial precursor cells after they undergo genetic alterations (i.e. EGFR amplification/mutation, PTEN loss/mutation, etc.) [82], thus primary rat post-natal day 2 astrocytes were used as the non-cancerous, healthy cells. While human astrocytes would be the ideal model to use, they are more difficult to obtain compared to rat astrocytes. In addition, as with human astrocytes, as adults get older, the astrocytes are more susceptible to undergo genetic mutations, and are therefore not a true representation of a healthy astrocyte. With astrocytes obtained from a post-natal rat pup, the likelihood of these genetic aberrations is further reduced. Therefore, rodent astrocytes are commonly used as a model for similar measurements in humans [83]. In addition, although human astrocytes are larger than rat astrocytes, when comparing the actin organization, both types observe F-actin organized in stress fibers [83, 84].

Average stiffness measurements and representative images for each cell type are shown in Figure 8. Astrocytes were significantly ($p<0.0001$) stiffer than each tumor cell type, with an average stiffness of 4184 ± 102.3 Pa. There was no statistical difference between the two GBM cell lines, U87MG and A172 tumor cells, which had an average stiffness of 1315 ± 39.98 Pa and 1138 ± 68.58 Pa, respectively. Primary GBM CICs, BT145, were statistically ($p<0.05$) less stiff than the primary astrocytes and the GBM tumor cell lines, with an average stiffness of 653.3 ± 35.37 Pa (Figure 8A). Finally, cytoskeletal stiffness of differentiated BT145s (dBT145) was 1308 ± 90.02 Pa (Figure 8B). Morphologies of the cells were also noticeably different between the various cell types (Figure 8C). Astrocyte morphology was more spread on the TCPS compared to the spindled morphology exhibited in the tumor cells.

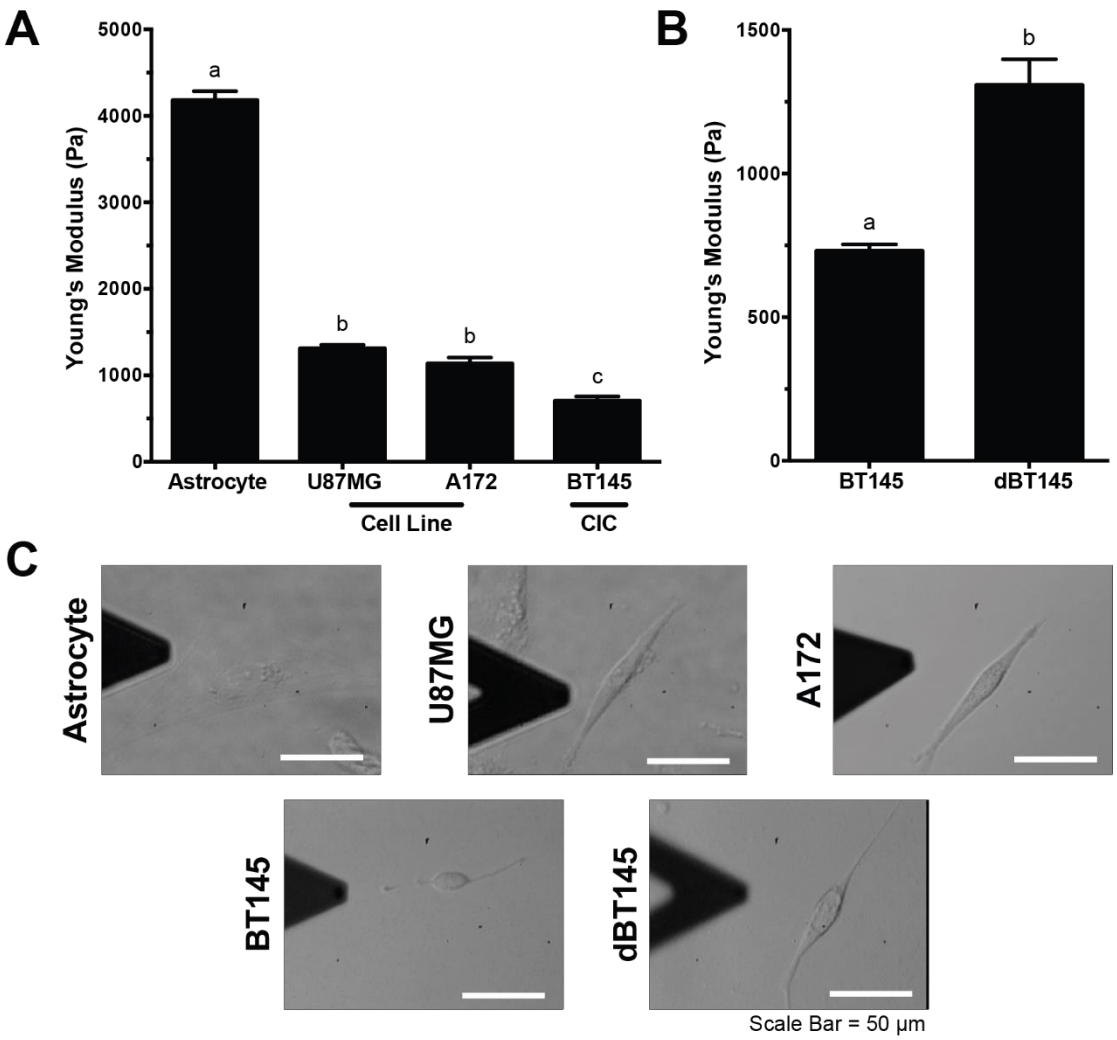

Figure 8: Cytoskeletal stiffness of cells decreases with increasing invasive potential. Atomic force microscopy was used to determine stiffness of primary astrocytes and GBM tumor cells when plated on collagen coated TCPS. A) Cytoskeletal stiffness of primary rat astrocytes, GBM cell lines, U87MG and A172, and primary GBM CICs, BT145. Analysis showed that GBM tumor cells were significantly softer than healthy astrocytes ($p<0.0001$). Further, highly invasive CICs were significantly less stiff than less invasive GBM cell lines ($p<0.05$). B) After differentiation of CICs with FBS, stiffness of cells significantly increased 2-fold ($p<0.01$). C) Representative brightfield images of astrocytes and tumor cells. N=3, mean ± SEM.

As a healthy cell undergoes oncogenic mutations, many cellular attributes are altered resulting in the abnormal growth and migratory behavior of cells [12]. Due to the role of the cytoskeleton on cell migration, previous studies identified biophysical attributes, specifically cytoskeletal stiffness, as a biomarker for invasive potential in a variety of cancers. Tumor studies using AFM to measure cytoskeletal stiffness have shown that more invasive breast, ovarian, and prostate cancer cells are less stiff than their less invasive or benign or healthy cell counterparts [16, 18, 24]. Significant 2-5 fold reductions in stiffness were observed between immortalized ovarian surface epithelial cells and different ovarian

cancer cell lines [18]. Similar results were observed in our experiments with the GBM tumor cells, as the highly invasive CICs were more compliant than the cancer cell lines U87MG and A172, which together, were significantly softer than non-cancerous astrocytes. During invasion, cancer cells need to deform their bodies in order to conform to the surrounding tissue in order to migrate. The reduced stiffness indicates a greater capability to deform within the aggressive tumor cells, which facilitates the migration and invasion through the surrounding ECM leading to secondary tumors [12].

5.1.2. Cellular Traction Forces Greater in Astrocytes than GBM Tumor Cells

Total cell traction force of the primary astrocytes, U87MG, A172, and BT145 were measured using traction force microscopy (TFM) (Figure 9). Cells were seeded on polyacrylamide gels overnight before being measured. For the primary astrocytes, a stiffer gel was used to measure the cell traction forces as the softer gels used for the tumor cells were too compliant and were pulled by the extremely contractile astrocytes, thus causing the beads to be in a different focal plane than the rest of the gel. This caused inaccurate measurements to be taken (data not shown). Therefore, a stiffer gel using 8% acrylamide and 0.1%-bis-acrylamide was used for the astrocytes. As the BT145s did not adhere well or generate traction on the aforementioned gel, a 5% acrylamide and 0.08%-bis-acrylamide gel was used for BT145. As gel stiffness influences traction force generated, U87MG and A172 cells were plated on both the 8% and 5% gel, and compared with the traction forces from the astrocytes and BT145s, respectively.

Figure 9A illustrates that non-cancerous astrocytes exerted significantly more cell traction force on the gel compared to the malignant GBM tumor cells. The average cell traction forces exerted by the astrocytes was 1240 ± 87.1 nN compared to the 129 ± 30.4 nN exerted by the malignant GBM tumor cells ($p<0.0001$). When comparing the traction forces of the cell lines and primary CICs, the A172 tumor cells exerted significantly greater force on the gel compared to BT145 cells, with an average cell traction force of 35.0 ± 9.41 nN and 5.60 ± 2.93 nN, respectively ($p<0.05$). However, a statistical difference was not observed between the U87MG tumor cells (14.6 ± 5.59 nN) and the A172s or BT145 tumor cells. Figure 9B displays representative stress maps of the cells. For the non-cancerous

astrocytes, the maximum traction stresses reach as high as 775 Pa; however, the maximum traction stresses of malignant tumor cells are an order of magnitude smaller.

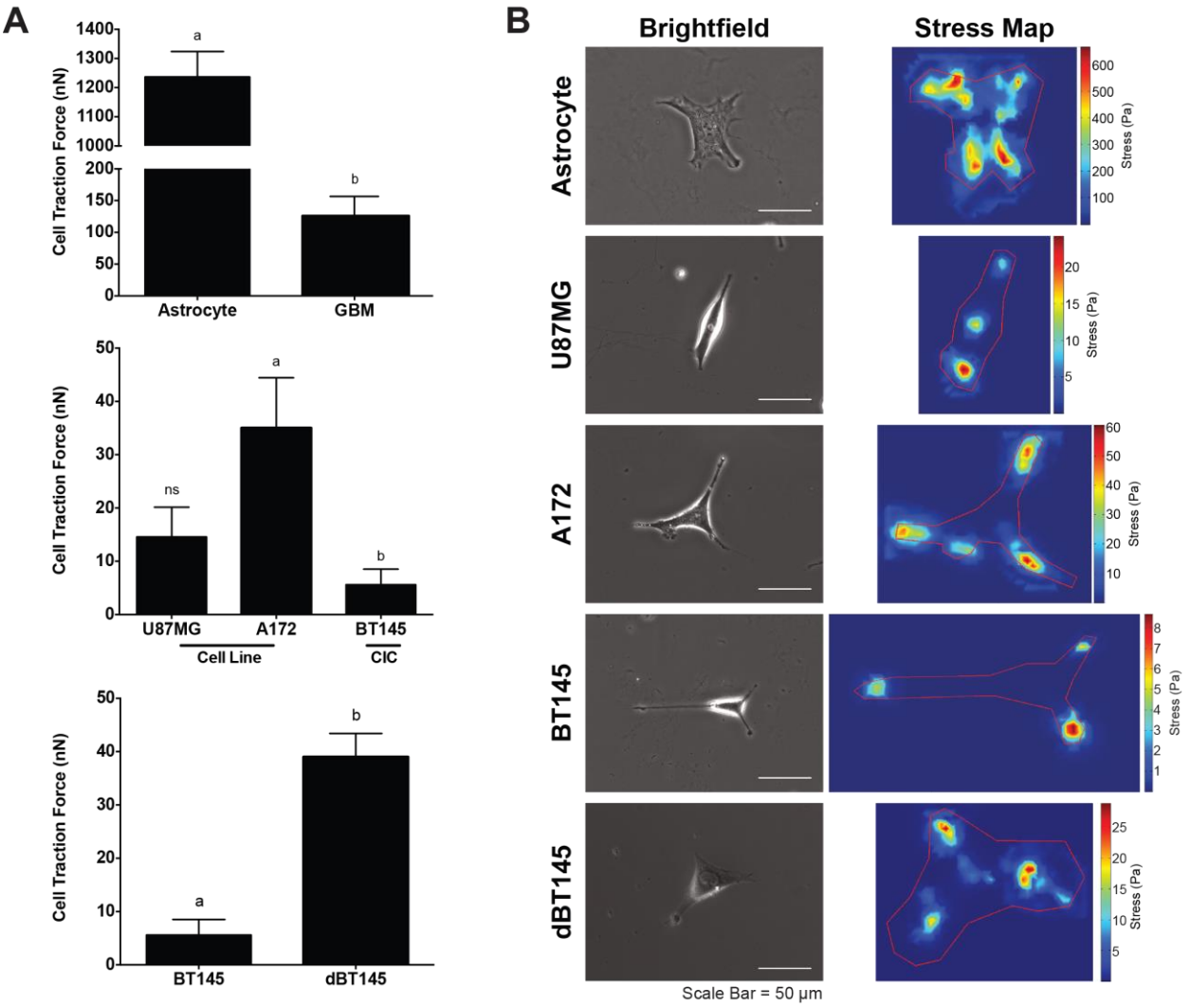

Figure 9: Cell traction forces decrease with increasing cell invasive potential. A) *Top panel:* TFM analysis demonstrated that traction forces between healthy astrocytes and GBM tumor cells significantly decrease ($p<0.0001$), nearly 98%. *Middle panel:* When GBM tumor cells are separated based on cell type, there was a significantly difference ($p<0.05$) in force generated between tumor cell line A172 and CICs, as CICs generated 84% less force than A172 cells. No differences were observed between U87MG tumor cells and other cells. *Bottom panel*: Upon differentiation of CICs, traction force significantly increases ($p<0.01$) when compared to their non-differentiated counterparts. B) Representative brightfield and stress maps of astrocytes and tumor cells. Stronger stresses are observed throughout the entire cell body of astrocytes. Weaker stresses, however, are observed on tumor cells. Furthermore, these stresses are primarily polarized. N=3, mean ± SEM.

Cellular traction forces, both total force and traction stresses, have also been investigated in other cancers to demonstrate how differing traction stresses can be correlative of invasive potential in cancer cells; however, conflicting results have been reported. Similar to what was observed in this study, an inverse relationship between

traction stress and cell metastatic potential in breast cancer cells and transformed fibroblasts was observed [70, 85]. However, other studies investigating breast, prostate, and lung cancer cells, showed that these cell types exerted significantly more total cell traction force than their non-metastatic counterparts [69]. One potential reason for the differing results is that traction forces are correlative with cell surface area and shape and the astrocytes observed in this study had a larger area than the GBM tumor cells. As a cell extends, traction forces play a key role in stretching the cell membrane and aid in maintaining contact with the substratum [86]. With high cell tension and a large area, the astrocytes cells likely form strong cell-matrix adhesions, thereby inhibiting migration.

5.1.3. Actin and Focal Adhesion Analysis of Astrocytes and GBM Tumor Cells Confirm that Invasive Potential is Associated with Reduced Focal Adhesion Presence

To determine if there were differences in cytoskeletal organization between astrocytes and malignant tumor cells, the cells were stained for vinculin (red), a focal adhesion protein, as well as F-actin (green) (Figure 10). The fluorescent images of the vinculin and F-actin co-stain can be seen in Figure 10A. Astrocytes exhibited aligned, densely-packed stress fiber networks distributed throughout the cell body, while actin distribution in GBM tumor cells appeared less dense. As marked differences were noted in focal adhesion formation, the percentage of positive vinculin area within a cell was quantified for the astrocytes and the GBM cell lines, U87MG, and A172. As astrocytes displayed a larger spreading area than the tumor cells, the ratio of vinculin area to cell area provides a reliable normalized measurement. As seen in Figure 10B, astrocytes exhibited significantly larger focal adhesion areas (22.51 ± 2.52%) than the U87MG (4.362 ± 1.12%) and A172 (12.50 ± 1.66%) tumor cells ($p<0.05$). A statistical difference was not observed in the percentage of positive vinculin area between the two GBM cell lines, U87MG and A172 tumor cells. This reduction in focal adhesion area also provides reason as to why the GBM tumor cells had weaker cell traction forces. The primary BT145 CICs were stained for vinculin and actin; however, observable amount of vinculin was not positively stained, which may be due to the CICs being a non-adherent tumor sub-population and vinculin not being localized to the focal adhesions.

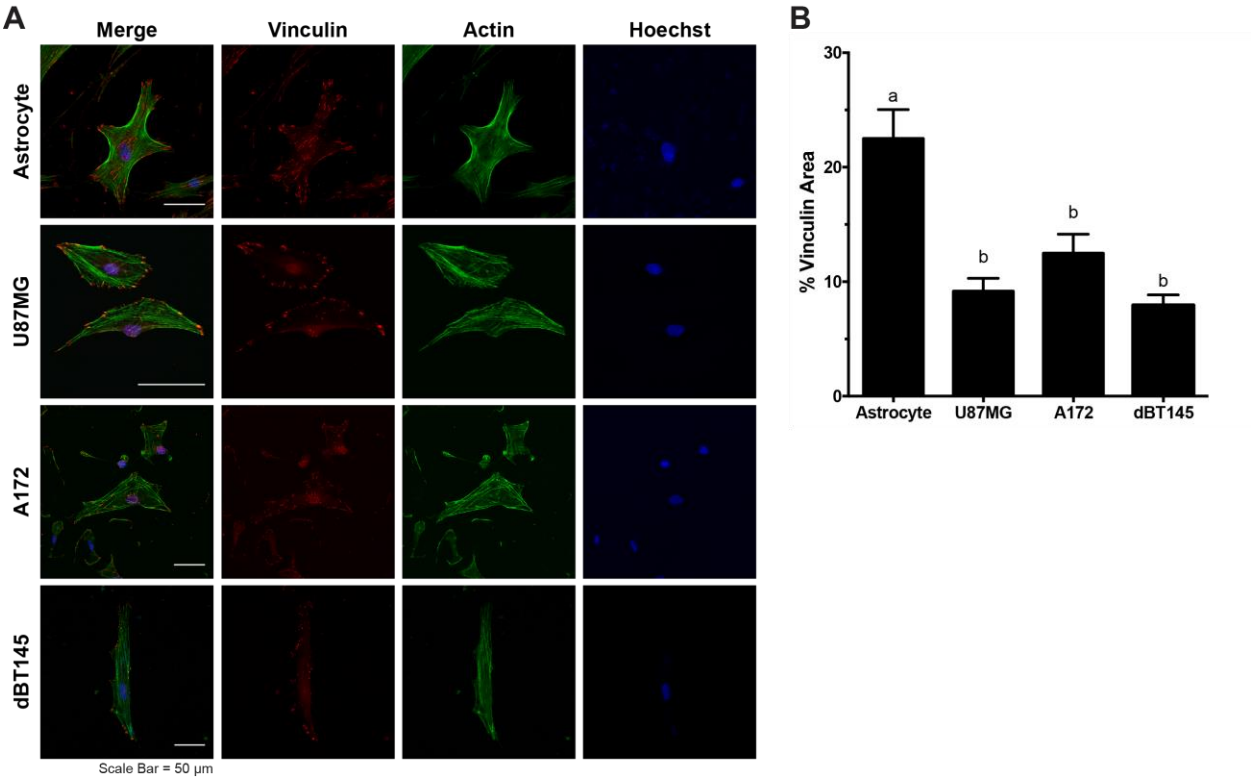

Figure 10: Cytoskeletal organization of astrocytes and tumor cells by staining for vinculin, a focal adhesion protein, and F-actin. A) Representative images of astrocytes and tumor cells of vinculin (red), F-actin (green), and counterstained with Hoechst (blue). Densely organized actin networks were observed in astrocyte cultures; however disorganized actin filaments were observed in U87MG and A172 tumor cell cultures. Further, vinculin was largely was localized throughout the entire cell body of astrocytes, however primarily localized to the periphery of tumor cells. B) Quantification of focal adhesions demonstrated that tumor cells resulted in significant reduction ($p<0.05$) in vinculin area/cell area compared to healthy astrocytes. N=3, mean ± SEM.

The differing biomechanical properties between the cancer and non-cancer cells are largely due to the changes in the cytoskeleton organization. Similar to what was observed in this study, it has been shown that non-malignant breast and ovarian cells formed a dense network of parallel actin filaments distributed throughout the cell body, however, their cancerous counterparts formed fewer filaments, most of which were shorter and largely disorganized, leading to the reduction in cytoskeletal stiffness [16, 18]. Focal adhesion complexes play a role in cell migration, as well as adhesion to the substratum. When focal adhesions attach and pull the surrounding ECM along the leading edge, traction forces are generated within the cell, moving the cell forward. In conjunction with focal adhesion formation, there must be a turnover of focal adhesion attachment at the trailing edge to allow for continuous directional cell migration [9]. Due to its role in migration, overexpression of vinculin has been shown to reduce cancer cell migration and invasion.

Conversely, a lack of vinculin expression has been associated with the development of many cancers, and potentially plays a role in epithelial-mesenchymal transition (EMT), thus suggesting a potential reason for the reduction of vinculin in the GBM cells [87].

5.1.4. Analysis of Biomechanical Properties Correlate CIC Differentiation with Decreased Invasive Capabilities

CICs, which are highly migratory and mainly responsible for tumor recurrence, are a key target for cancer therapies. As these cells are resistant to traditional chemotherapeutic strategies, differentiation therapy is being developed as an approach to treat GBM tumors to inhibit their stem-like phenotype thereby reducing tumorigenicity. By treating stem-like glioma cells with all-trans retinoic acid-containing medium to induce differentiation, Campos *et al.* showed a decrease in cellular invasion [88]. While the majority of other studies focus on the biochemical mechanism of CIC differentiation, we investigated the effect of differentiation on the biophysical properties of these cells.

To determine if the difference in biophysical properties between the GBM cells lines and the GBM CICs was due to differentiation, the BT145 CICs were differentiated using media without EGF or FGF, but containing 10% FBS for 3 weeks. Following differentiation, the cytoskeletal stiffness, traction force, and percent of positive vinculin area were measured. The cytoskeletal stiffness of the differentiated BT145 (dBT145) tumor cells significantly increased to 1310 ± 90.0 Pa ($p<0.01$), similar to that of the U87MG and A172 tumor cell lines (Figure 8B). In addition, the cell traction forces of the dBT145s (39.03 ± 4.384 nN) were measured and the traction forces significantly increased ($p<0.01$) compared to the primary BT145 tumor cells (Figure 9). Finally, positive vinculin staining was quantified, and contrary to their non-differentiated counterparts, the dBT145 tumor cells adhered well onto the surface with observed stress fiber formation and had a similar percentage of positive vinculin area (7.93 ± 0.92%) as the U87MG and A172 tumor cells (Figure 10).

Moreover, cell morphologies between dBT145s and their non-differentiated counterparts were observably distinct. After differentiation, cytoskeletal stiffness, cell traction force, and percent of positive vinculin area significantly increased compared to

their undifferentiated CIC counterparts. In addition, these properties were similar to that of the less invasive cancer cell lines U87MG and A172, supporting that differentiation leads to a less invasive phenotype. Therefore, this supports previous reports that state CICs have a more invasive potential than differentiated tumor cells [88-90].

5.2. Specific Aim 2

5.2.1. Cytoskeletal Stiffness Analysis of Cells on Aligned Nanotopography Corroborates that Stiffness is Correlative of Invasive Potential

The measurement of cytoskeletal stiffness on a rigid 2D substrate provides important baseline characteristics of the cells; however it is important to measure these values on a scaffold that mimics the *in vivo* tumor microenvironment to obtain more biologically relevant results. Therefore, we used polycaprolactone (PCL) substrates (smooth film, randomly aligned nanofibers, and aligned nanofiber films) to investigate whether cell biomechanical properties would change. The nanofibers mimic the nanotopographical cues provided by the white matter tracts and blood vessels in the *in vivo* tumor microenvironment. Electrospun nanofibers have been previously used as a model for glioblastoma and breast cancer migration [21, 22, 76, 77].

As GBM tumor cells migrate along white matter tracts and blood vessels, we used aligned PCL nanofibers to mimic these biological substrates, as well as randomly aligned nanofibers, and smooth film to observe if there was a difference in the cell behavior. By using a rotating mandrel, aligned nanofibers with an average diameter of 668 ± 98.6 nm were fabricated, within the range of diameters of white matter tracts observed in the human brain. While the diameters of these topographic substrates range from person to person (from 0.3 μm to 10 μm [91]), on average, median and average white matter tract diameters have been shown to be below 1 μm [92]. Randomly aligned nanofibers had an average diameter of 621 ± 173 nm. Degrees of alignment for aligned and randomly aligned nanofibers were 3.1 ± 2.3 degrees and 46.8 ± 54.8 degrees, with the positive y-axis being 0 degrees. SEM images of the different substrates can be seen in Figure 11A. The difference in alignment can be observed between the aligned and the randomly aligned nanofibers films. By using aligned nanofibers, randomly aligned nanofibers and a smooth, non-

topographic film, we were able to investigate how nanotopography and fiber orientation affected cell behavior.

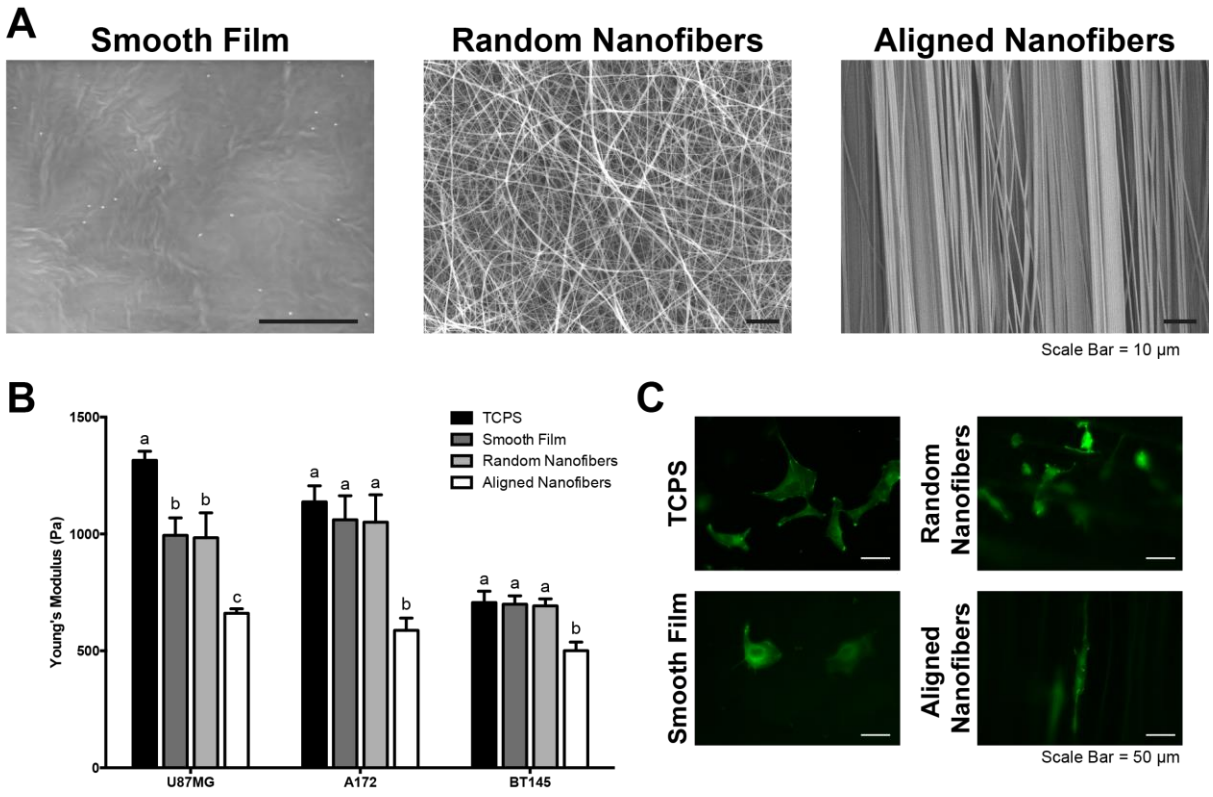

Figure 11: Aligned nanotopography resulted in decreased cytoskeletal stiffness. A) Electrospinning was used to fabricate randomly aligned and aligned nanofibers of 621 ± 173 nm and 668 ± 98.6 nm, respectively. Lack of surface nanotopography is observed in smooth film. B) AFM was used to determine cytoskeletal stiffness of tumor cells when cultured on differing nanotopographic substrates. When cultured on aligned nanofibers, cytoskeletal stiffness significantly decreased ($p<0.05$) compared to each other substrate for each cell type. C) Representative fluorescent images of A172-GFP-actin tumor cells on different substrates. N=3, mean ± SEM.

In order to determine the effect of nanotopography on cytoskeletal stiffness, AFM was used to measure the cytoskeletal stiffness of U87MG, A172, and BT145 tumor cells seeded on collagen coated TCPS, smooth film, randomly aligned nanofibers, and aligned nanofibers (Figure 11B). For both cell lines and CICs, the cytoskeletal stiffness was significantly smaller on the aligned nanofibers ($p<0.05$) compared to both randomly aligned nanofibers and smooth film with stiffness measurements of 995 ± 74.2 Pa, 984 ± 107 Pa, and 661 ± 18.5 Pa, for the U87MG cells on the smooth film, randomly aligned nanofibers, and aligned nanofibers, respectively. Stiffness for U87MG tumor cells cultured on the aligned nanofibers decreased 2-fold compared to TCPS and about 1.5-fold compared to the other substrates. Similar trends in stiffness were also observed for A172 and BT145

tumor cells. Representative fluorescent images of cells on each substrate can be seen in Figure 11C.

It has been shown previously that cells cultured on aligned nanofibers migrate further and up to five times faster than on randomly aligned nanofibers or substrates without nanotopography, similar to tumor cell migration speeds *in vivo* [21, 76, 78]. Together, with the earlier data that showed that cytoskeletal stiffness is a biomarker for GBM invasive potential, we see that the more invasive a cell is, the more compliant it is. The actin cytoskeleton is undergoing rapid depolymerization and polymerization during migration, which likely leads to the reduced stiffness [93]. In addition, Rosa-Cusachs *et al*. investigated how the elongated cell shape affects the actin cytoskeleton and reduced cytoskeletal stiffness in endothelial cells [94]. They suggest that the spatial organization of the actin cytoskeleton of elongated cells is part of the reason of a reduced cytoskeletal stiffness, due to the reduction of crosslinking in parallel actin networks compared to a densely crosslinked network of spread cells [94]. This data highlights that an aligned nanotopography has the ability to alter cytoskeletal stiffness, thereby promoting a more migratory cell state.

Previously MacKay *et al.* investigated the effects of genetically manipulating glioma cells by delivering constitutively active RhoA to determine the effect on the cell's mechanical properties. It was found that increasing constitutively active RhoA expression led to increased traction forces and decreased cell migration speeds. This reduction in migration was likely due to the cells adhering too strongly to the substratum [95]. However, investigating the mechanical properties by mimicking the nanotopography of the blood vessels and white matter tracts has not been investigated.

5.2.2. Nanotopography and Alignment Correlates with Enhanced Migratory and Reduced Proliferative Phenotype in Tumor Cells

With the effect of nanotopography on the biomechanical attributes of cells investigated, further analysis on gene expression along the migratory signaling pathways was completed using qRT-PCR. Gene expression analysis was completed for pro-migratory gene markers zinc finger protein SNAI1 (SNAI1) and Notch homolog 1 (NOTCH1), anti-

migratory gene marker reversion-inducing-cysteine-rich protein with kazzal motifs (RECK), and pro-proliferative gene markers cyclin-dependent kinase 20 (CDK20) and cyclin D1 (CCND1). U87MG and A172 tumor cells exhibited greater than ± 2 fold changes for all of the investigated genes when seeded on the aligned nanofibers compared to TCPS (Figure 12). The fold increase on the aligned nanofibers compared to TCPS for pro-migratory SNAI1 and NOTCH1 markers was 10.12 and 3.39 for U87MG tumor cells, and 16.75 and 3.09 for A172 tumor cells, respectively. Anti-migratory RECK was downregulated 3.10 and 3.83 fold in the U87MG and A172 tumor cells, respectively.

Pro-proliferative gene markers CDK20 and CCND1 were also downregulated 2.72 and 2.02 fold compared to TCPS for U87MG cells. Similar decreased gene expression was observed in A172 tumor cells, with 2.99 and 2.54 fold respective downregulation. Furthermore, there were statistical differences between the aligned nanofiber films and the smooth film substrate for all of the analyzed genes. When comparing the gene expression of the A172 tumor cells on aligned nanofibers and randomly aligned nanofibers for NOTCH1, a greater than 2-fold difference was observed. However, for the U87MG cells on the aligned nanofibers and randomly aligned nanofibers, a greater than 2-fold expression difference was observed for the expression of SNAI1.

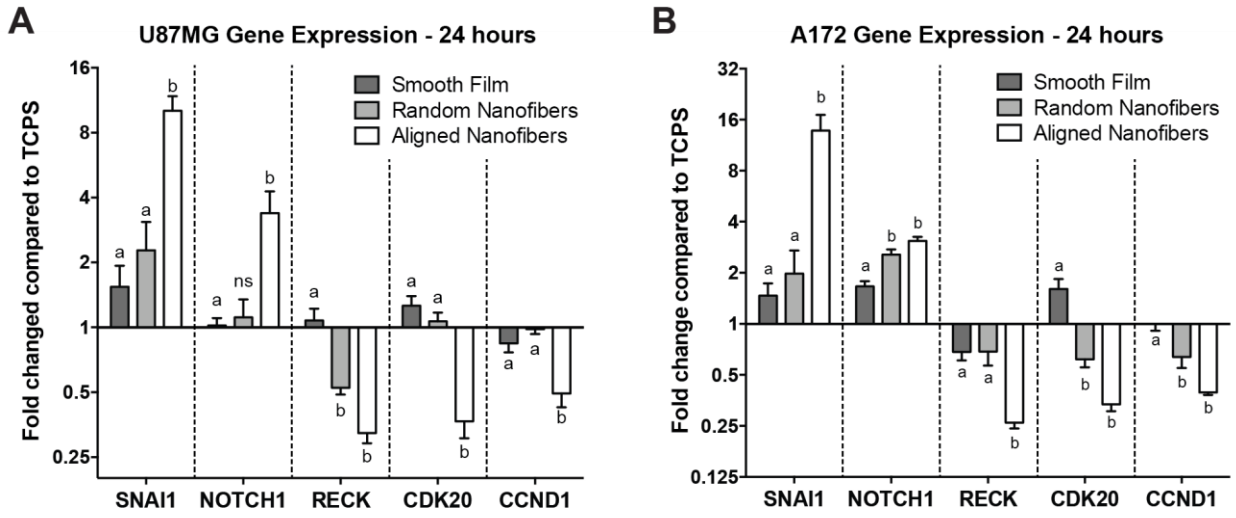

Figure 12: Aligned nanotopography resulted in the most significant increase in pro-migratory and decrease in pro-proliferative gene markers. Quantitative real time PCR for gene expression in U87MG (A) and A172 (B) cells when plated on TCPS, smooth film, randomly aligned nanofibers, and aligned nanofibers for 24 hours. Results are shown with fold expression relative to the TCPS condition. Aligned nanotopography resulted in the significant upregulation of pro-migratory marker SNAI1 and NOTCH1, downregulation of anti-migratory marker RECK, and decreased pro-proliferative markers CDK20 and CCND1 ($p<0.05$). N=3, mean ± SEM.

Previous studies have shown culturing of GBM tumor cells on aligned chitosan-PCL fibers of 200 and 400 nm resulted in the significant upregulation of several migratory and EMT gene markers [76]. Our data demonstrated a significant increase of SNAI1 and NOTCH1 expression on the aligned nanofibers. Notch signaling has been shown to promote EMT through regulation of SNAI1 [42, 43]. Zhang *et al*. showed that elevation of NOTCH1 signaling in GBM cells and in tumor biopsies led to increased tumor invasion and EMT markers expression [41]. Downregulation of metastasis suppressor RECK, which was observed on the aligned nanofibers, is essential for the invasiveness in GBM cells, as overexpression of RECK in T98G glioblastoma tumor cells altered the cytoskeleton to produce fewer lamellipodia and greater stress fibers, indicating decreased mobility [48].

In addition, we also investigated the effect of substrate nanotopography on genes responsible for proliferation. GBM tumors have exhibited a "go-or-grow" phenomenon in which there is a dichotomy between the migratory (go) and proliferative (grow) behavior of the tumor cells. Previous studies have shown that invading cells at the leading edge of the tumor have low proliferative index by inhibiting entry into the cell cycle, while cells located in the tumor core are highly proliferative, *in vitro* and *in vivo* [53, 55-57]. Using an implantable nanofiber film to direct tumor cell migration, Jain *et al*. showed that cells migrating away from the tumor core were in a less proliferative state on the aligned nanofibers compared to a smooth film control, as suggested with the reduced Ki67 staining. F-actin staining analysis showed that cells grown on the aligned nanofiber film exhibited uniform F-actin filaments compared to more punctate F-actin staining of cells on a smooth film, suggesting a less migratory, suspended state on the smooth film [21]. Gene expression of CDK20 and CCND1, both of which play a role in the transition from the G1/S phase in the cell cycle, were significantly downregulated on the aligned nanofibers, with a greater than 2-fold decrease compared to the TCPS control, further purporting that substrate nanotopography induces a propensity for a migratory GBM tumor cell state [50, 96].

5.2.3. Aligned Nanotopography Promotes Tumor Cells to be in G1 Phase of Cell Cycle

To further investigate how substrate nanotopography affects cell state, cell cycle analysis by DNA content was completed using flow cytometry. As shown in Figure 13 cells

on the aligned fibers had a significantly greater population of cells in the G1 phase than when grown on non-topographic TCPS ($p<0.05$, 71.3 ± 0.9% versus 65.4 ± 1.1%, respectively); however, no statistical differences were observed between any other groups, with 66.8 ± 0.3% and 67.1 ± 1.4% cells being in the G1 phase on the smooth film and randomly oriented nanofiber substrates, respectively. In addition, there was a significant reduction ($p<0.01$) in population of cells in the S phase when cultured on aligned nanofibers (8.9 ± 0.8%) compared to when cultured on smooth film (13.8 ± 0.3%). No significant differences in the S phase were observed between these groups and cells grown on TCPS (12.0 ± 0.8%) and randomly aligned nanofibers (12.1 ± 1.1%). Interestingly, no significant differences in percent population in the G2/M phase were observed between any group, with 22.7 ± 1.2%, 19.4 ± 0.3%, 20.8 ± 0.4%, and 19.8 ± 1.3% in the G2/M phase on TCPS, smooth film, randomly aligned nanofibers, and aligned nanofibers, respectively.

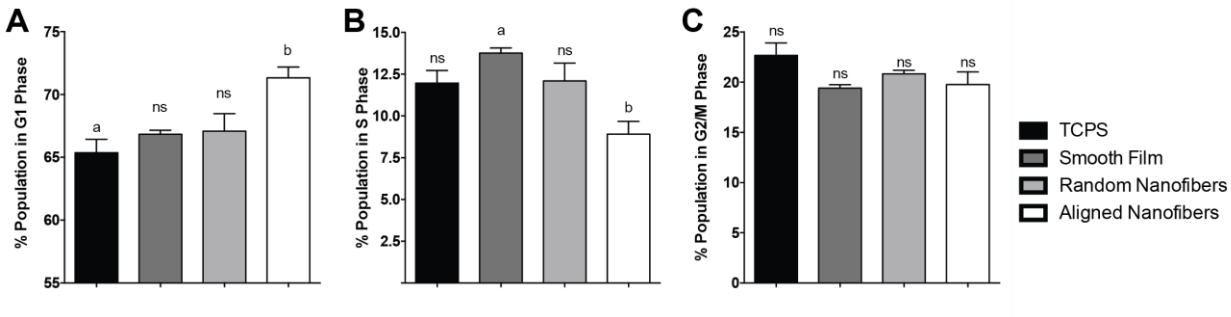

Figure 13: Cell cycle analysis by DNA content for tumor cells on TCPS, smooth film, randomly aligned, and aligned nanofibers showed aligned nanotopography promotes enhanced population in the G1 phase of the cell cycle. Analysis of FACS histograms of population of cells in the (a) G1 phase, (b) S phase, and (c) G2/M phase of the cell cycle. Analysis shows that there is a significant increase in cells in the G1 phase of the cell cycle on the aligned nanofibers compared to TCPS. N=3, mean ± SEM.

These data support the earlier gene expression analysis that the cells on the aligned nanofibers are less in a proliferative phase due to the increase of population in the G1 phase of the cell cycle. In addition, similar results have been previously reported in gastric cancer cells cultured in Gelfoam® histoculture to mimic metastasis. It was found invading cancer cells were predominantly in the G0/G1 phase of the cell cycle instead of S/G2/M phases. In addition, they found cells in the G0/G1 migrated faster and further than cells in the proliferative phases, and upon entering the S-phase, migration ceased until mitosis finished [97]. One benefit of this study compared to our study is cell phase at the tumor

periphery and core were quantified separately, thus minimizing confounding effects of the highly proliferative tumor core.

5.2.4. Morphometric Analysis of Focal Adhesions Correlate Larger, Elongated Adhesions with a Migratory State

The cytoskeletal organization of cells on glass, randomly aligned nanofibers, and aligned nanofibers was analyzed to further describe the effect of nanotopography on the cytoskeleton. As seen in Figure 14, cells on the aligned nanofibers formed parallel actin filaments along the direction of the fibers. In addition, clusters of focal adhesions can be observed along the poles of these cells. Cells on randomly aligned fibers observed a randomly spread morphology, forming extensions in different directions along the fibers. Individual vinculin adhesions were characterized by area, length, and shape factor (Figure 14B). Focal adhesions on the aligned nanofibers were significantly larger in area and length than the adhesions on glass or randomly aligned nanofibers. Focal adhesion areas on aligned nanofibers, randomly aligned nanofibers, and glass were $5.74 \pm 0.441\ \mu m^2$, $3.91 \pm 0.268\ \mu m^2$, and $2.96 \pm 0.209\ \mu m^2$ respectively. In addition, adhesions also had a significantly smaller shape factor ($4\pi(\text{area})/(\text{perimeter})^2$) on the aligned nanofibers (0.63 ± 0.020), indicating that the adhesions exhibited a more elongated, elliptical shape than those cultured on glass (0.76 ± 0.17) and randomly aligned nanofibers (0.81 ± 0.012).

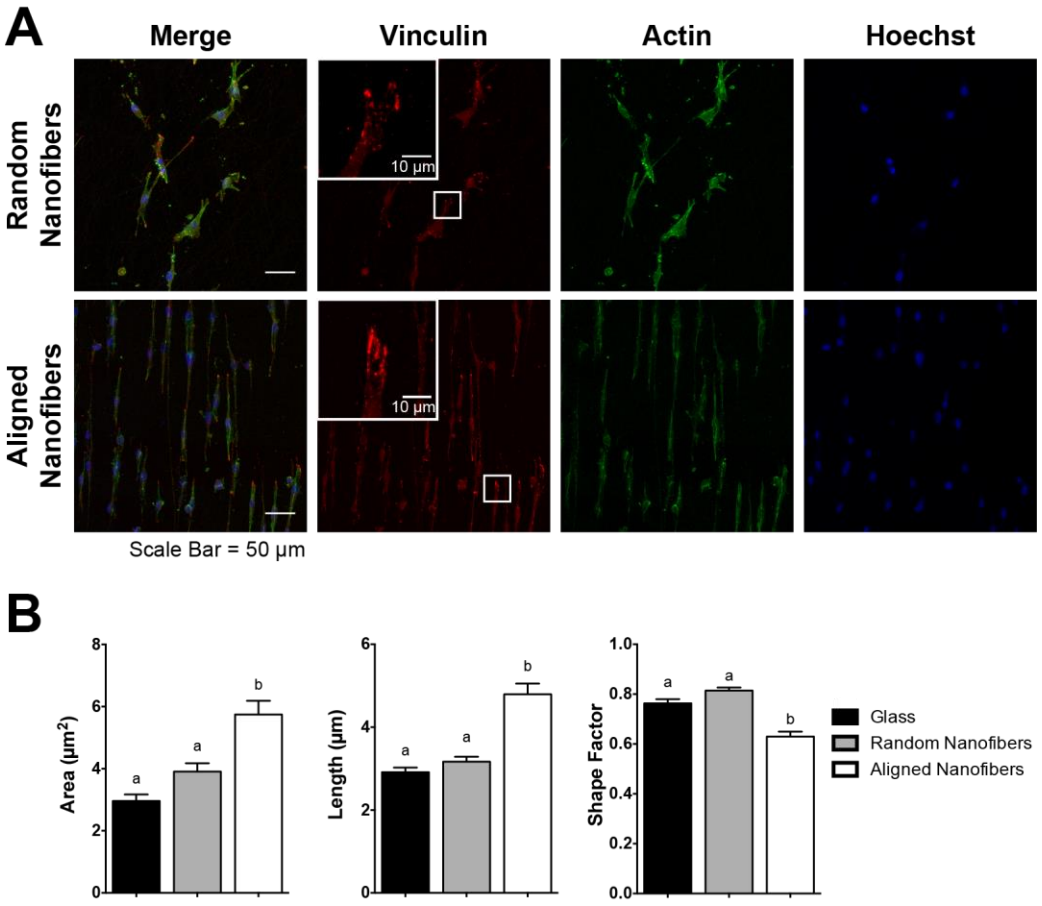

Figure 14: Aligned nanotopography promotes larger and more elongated focal adhesions. A) Representative images of U87MG tumor cells of vinculin (red), F-actin (green), and counterstained with Hoechst (blue) on aligned and randomly aligned nanofibers. White box highlights a magnified area in the inset for the fluorescent images showing vinculin staining. Aligned nanofibers promoted a spindled morphology, while randomly aligned nanofibers exhibited cells with multiple processes along the fiber directions. B) Quantification and analysis of vinculin adhesions showed that cells on aligned nanofibers had adhesions that were significantly larger in area, longer, and more elliptical ($p<0.001$) then when on randomly aligned fibers or glass. N=21, mean ± SEM

Substrate and ECM nanotopography have an effect on stress fiber and focal adhesion formation. Human mesenchymal stem cells cultured on 500 nm gratings of TCPS exhibited increased vinculin protein expression compared to unpatterned controls. In addition, the cells on the nanotopographic substrates exhibited a reduction in cytoskeletal stiffness and an elongated morphology with an aligned actin cytoskeleton and a dense focal adhesion population around the poles of the cells, compared to adhesions localized to both the central and peripheral region on cells on unpatterned substrates [10]. Similar results were found across a variety of cell types including epithelial, kidney, and fibroblast cells [36-38].

In addition, Kim *et al*. investigated the effects of individual focal adhesion size on cell motility in mouse embryonic fibroblasts. While a moderately correlative inverse linear

relationship was found between shape factor and cell migration speed, they found that focal adhesion size was highly predictive of cell speed [98]. Similar results were also observed with C2C12 mouse myoblast cells cultured on aligned suspended nanofibers. These cells exhibited higher migration speeds, with focal adhesion clusters approximately 4x times longer than when grown on a non-topographic substrate. An increased presence of longer filopodia along the lamellipodial leading edge have been observed on cells on an aligned topography, and likely aid in enhancing the migration speed [99]. Together, this suggests the aligned nanotopography provides the guidance cues necessary to reorganize the cytoskeleton to promote a propensity for a migratory state.

CHAPTER 6: FUTURE WORK AND CONCLUSIONS

6.1. FUTURE WORK

Studying the biomechanical properties as a biomarker for invasive potential has been studied previously in other cancers however has yet to be reported in GBM. While this study used astrocytes as a healthy control, GBM is also believed to possibly arise from glial precursor cells and neural stem cells. In addition, while the majority of GBM arises from the *de novo* pathway (through astrocytes, glial precursor cells, or neural stem cells), GBM can also arise through the progression of lower grade astrocytomas. This study just focused on GBM cell lines and highly invasive CICs, thus there is a large gap between healthy cells and Grade IV astrocytoma cells. Therefore, using additional controls of neural stem cells and low grade or benign brain tumors, such as pilocytic astrocytomas, a more comprehensive analysis of using cell stiffness or traction forces as a biomarker for invasive potential could be completed. In addition, it may provide answers for the conflicting traction force results observed in this study compared to other cancers.

Further, while this study set the groundwork for the *in vitro* model and identified biomechanical differences between the cells on the aligned nanofibers, moving forward, we would like to elucidate the mechanism that leads to the enhanced migratory cell state. This model can be used to monitor what is happening *in vivo* at a faster rate with more biologically relevant results than on previously used models. In order to investigate potential mechanisms, cells can be transduced to identify proteins of interest, and then plated onto these nanofiber films and placed into a live imaging chamber. This will allow for quantification of protein trafficking within the cell that plays a role in migration. In addition, by using a live imaging chamber, vinculin, or other focal adhesion proteins, and F-actin can be fluorescently tagged to exhibit cytoskeletal dynamics during migration on these substrates. By identifying the mechanism involved in the altering gene and protein expression, more effective therapies can be developed to inhibit the infiltrative nature of these cells.

Additionally, one aspect that was not investigated in this study was the nanofiber material, as here, only collagen coated PCL nanofibers were used. As PCL is a synthetic polymer and is not comparable to the mechanical or chemical properties of the white matter tracts or blood vessels, electrospinning hyaluronic acid or collagen nanofibers could be used to create a model more mimetic of the migratory paths. It has been previously shown that spinning a PCL core with an HA or collagen shell affected the initial attachment, cell stretching, and migration rate of GBM tumor cells, thus surface chemistry is just as important as the physical nanotopography of the substrate [77].

Unfortunately, due to technical limitations, the gene expression analysis was not completed on the primary CICs. While attempts were made to collect RNA from these samples, they were unsuccessful due to low yields and poor 260/280 ratios. Therefore, more optimization would need to be completed in order to obtain gene expression on the CICs when plated on the nanofiber substrates. Once optimized, it would of interest to see if conventional CIC markers (CD133, nestin, etc.) are regulated by nanotopographical patterning as well. In addition, protein expression analysis via western blotting of migratory and proliferative markers could also be completed to further support the claims suggested in this study.

6.2. Broader Applications and Implications

While the work presented here was focused on GBM, the nanofiber model has broader applications and can be used as a research tool for cancer cell migration [3]. Nanofibers have already been used to study breast cancer cell migration, however it can also be applied to other highly invasive cancers, such as pancreatic cancer, to help elucidate the migratory mechanism. Identifying the migratory mechanism responsible for the enhanced invasive nature of these diseases will help researchers identify gene or protein targets for therapies to minimize invasion.

Further, due to the heterogeneity of GBM, not all treatments will work across all patients. With this *in vitro* model, researchers can quickly monitor what is happening *in vivo* on a microscopic scale. The aligned nanofibers can be used as an *in vitro* diagnostic

tool for tumor biopsies to complete genotype/phenotype analysis, and provide drug screening for development of personalized treatment therapies.

6.3. CONCLUSION

This study investigated the biomechanical properties of highly aggressive and migratory GBM tumor cells. We demonstrate that the cytoskeletal stiffness, traction forces, and focal adhesion formation is significantly reduced in the highly invasive tumor cells compared to healthy astrocytes. In addition, by using an aligned nanofiber film that mimics the white matter tracts and blood vessels highways for cell migration, we observed a reduction in cytoskeletal stiffness likely due to the reduction in crosslinking in an aligned actin cytoskeleton. Together, with the upregulation of migratory related genes on the aligned nanofibers, aligned actin cytoskeleton, and increased presence of larger, elongated adhesions, these data suggest the aligned nanotopography promotes the biophysical changes in the cells leading to an enhanced migratory state, as shown in Figure 15 . Testing the biomechanical properties of GBM is an effective diagnostic methodology to determine the aggressiveness of GBM tumor. This *in vitro* model can further be applied to elucidate how the nanotopography of the substrates transduces into altered gene and protein expression to induce tumor cell invasion and migration, thus providing a mechanism to inhibit the process to form secondary tumor sites.

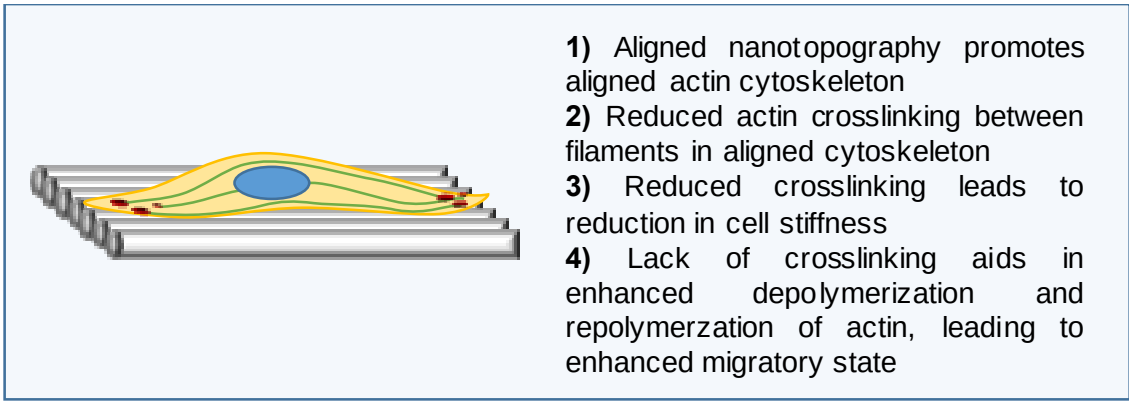

Figure 15: Graphical conclusion of enhanced migratory state of GBM tumor cells the aligned nanofibers

REFERENCES

1. Ostrom, Q.T., et al., *CBTRUS statistical report: primary brain and central nervous system tumors diagnosed in the United States in 2007-2011.* Neuro Oncol, 2014. **16 Suppl 4**: p. iv1-63.
2. Stupp, R., et al., *Radiotherapy plus concomitant and adjuvant temozolomide for glioblastoma.* N Engl J Med, 2005. **352**(10): p. 987-96.
3. Agnihotri, S., et al., *Glioblastoma, a brief review of history, molecular genetics, animal models and novel therapeutic strategies.* Arch Immunol Ther Exp (Warsz), 2013. **61**(1): p. 25-41.
4. Eyler, C.E. and J.N. Rich, *Survival of the fittest: cancer stem cells in therapeutic resistance and angiogenesis.* J Clin Oncol, 2008. **26**(17): p. 2839-45.
5. Bellail, A.C., et al., *Microregional extracellular matrix heterogeneity in brain modulates glioma cell invasion.* Int J Biochem Cell Biol, 2004. **36**(6): p. 1046-69.
6. Holland, E.C., *Glioblastoma multiforme: the terminator.* Proc Natl Acad Sci U S A, 2000. **97**(12): p. 6242-4.
7. Hall, A., *Rho GTPases and the actin cytoskeleton.* Science, 1998. **279**(5350): p. 509-14.
8. Provenzano, P.P. and P.J. Keely, *Mechanical signaling through the cytoskeleton regulates cell proliferation by coordinated focal adhesion and Rho GTPase signaling.* J Cell Sci, 2011. **124**(Pt 8): p. 1195-205.
9. Nagano, M., et al., *Turnover of focal adhesions and cancer cell migration.* Int J Cell Biol, 2012. **2012**: p. 310616.
10. Yim, E.K., et al., *Nanotopography-induced changes in focal adhesions, cytoskeletal organization, and mechanical properties of human mesenchymal stem cells.* Biomaterials, 2010. **31**(6): p. 1299-306.
11. Mikheeva, S.A., et al., *TWIST1 promotes invasion through mesenchymal change in human glioblastoma.* Mol Cancer, 2010. **9**: p. 194.
12. Suresh, S., *Biomechanics and biophysics of cancer cells.* Acta Biomater, 2007. **3**(4): p. 413-38.
13. Lamouille, S., J. Xu, and R. Derynck, *Molecular mechanisms of epithelial-mesenchymal transition.* Nat Rev Mol Cell Biol, 2014. **15**(3): p. 178-96.
14. Corbin, E.A., et al., *Biophysical properties of human breast cancer cells measured using silicon MEMS resonators and atomic force microscopy.* Lab Chip, 2015. **15**(3): p. 839-47.
15. Lekka, M., et al., *Cancer cell detection in tissue sections using AFM.* Arch Biochem Biophys, 2012. **518**(2): p. 151-6.
16. Li, Q.S., et al., *AFM indentation study of breast cancer cells.* Biochem Biophys Res Commun, 2008. **374**(4): p. 609-13.
17. Ramos, J.R., et al., *The softening of human bladder cancer cells happens at an early stage of the malignancy process.* Beilstein J Nanotechnol, 2014. **5**: p. 447-57.
18. Xu, W., et al., *Cell stiffness is a biomarker of the metastatic potential of ovarian cancer cells.* PLoS One, 2012. **7**(10): p. e46609.
19. Swaminathan, V., et al., *Mechanical stiffness grades metastatic potential in patient tumor cells and in cancer cell lines.* Cancer Res, 2011. **71**(15): p. 5075-80.
20. Cross, S.E., et al., *Nanomechanical analysis of cells from cancer patients.* Nat Nanotechnol, 2007. **2**(12): p. 780-3.
21. Jain, A., et al., *Guiding intracortical brain tumour cells to an extracortical cytotoxic hydrogel using aligned polymeric nanofibres.* Nat Mater, 2014. **13**(3): p. 308-16.
22. Nelson, M.T., et al., *Preferential, enhanced breast cancer cell migration on biomimetic electrospun nanofiber 'cell highways'.* BMC Cancer, 2014. **14**: p. 825.
23. Leung, M., et al., *Nanofiber-based in vitro system for high myogenic differentiation of human embryonic stem cells.* Biomacromolecules, 2013. **14**(12): p. 4207-16.
24. Faria, E.C., et al., *Measurement of elastic properties of prostate cancer cells using AFM.* Analyst, 2008. **133**(11): p. 1498-500.
25. Goldbrunner, R.H., J.J. Bernstein, and J.C. Tonn, *Cell-extracellular matrix interaction in glioma invasion.* Acta Neurochir (Wien), 1999. **141**(3): p. 295-305; discussion 304-5.
26. Altaner, C., *Glioblastoma and stem cells.* Neoplasma, 2008. **55**(5): p. 369-74.

27. Romaguera-Ros, M., et al., *Cancer-initiating enriched cell lines from human glioblastoma: preparing for drug discovery assays.* Stem Cell Rev, 2012. **8**(1): p. 288-98.
28. Fletcher, D.A. and R.D. Mullins, *Cell mechanics and the cytoskeleton.* Nature, 2010. **463**(7280): p. 485-92.
29. Cooper, G.B., *The Cell: A Molecular Approach*. 2nd Edition ed, ed. Sunderland. 2000, Boston: Sinauer Associates.
30. Wehrle-Haller, B. and B.A. Imhof, *Actin, microtubules and focal adhesion dynamics during cell migration.* Int J Biochem Cell Biol, 2003. **35**(1): p. 39-50.
31. Quail, D.F. and J.A. Joyce, *Microenvironmental regulation of tumor progression and metastasis.* Nat Med, 2013. **19**(11): p. 1423-37.
32. Carman, C.V. and T.A. Springer, *Integrin avidity regulation: are changes in affinity and conformation underemphasized?* Curr Opin Cell Biol, 2003. **15**(5): p. 547-56.
33. Turner, C.E., *Paxillin interactions.* J Cell Sci, 2000. **113 Pt 23**: p. 4139-40.
34. Owens, L.V., et al., *Overexpression of the focal adhesion kinase (p125FAK) in invasive human tumors.* Cancer Res, 1995. **55**(13): p. 2752-5.
35. Sieg, D.J., C.R. Hauck, and D.D. Schlaepfer, *Required role of focal adhesion kinase (FAK) for integrin-stimulated cell migration.* J Cell Sci, 1999. **112 (Pt 16)**: p. 2677-91.
36. Britland, S., et al., *Synergistic and hierarchical adhesive and topographic guidance of BHK cells.* Exp Cell Res, 1996. **228**(2): p. 313-25.
37. den Braber, E.T., et al., *Orientation of ECM protein deposition, fibroblast cytoskeleton, and attachment complex components on silicone microgrooved surfaces.* J Biomed Mater Res, 1998. **40**(2): p. 291-300.
38. Teixeira, A.I., et al., *Epithelial contact guidance on well-defined micro- and nanostructured substrates.* J Cell Sci, 2003. **116**(Pt 10): p. 1881-92.
39. Ananthanarayanan, B., Y. Kim, and S. Kumar, *Elucidating the mechanobiology of malignant brain tumors using a brain matrix-mimetic hyaluronic acid hydrogel platform.* Biomaterials, 2011. **32**(31): p. 7913-23.
40. Mahesparan, R., et al., *Extracellular matrix-induced cell migration from glioblastoma biopsy specimens in vitro.* Acta Neuropathol, 1999. **97**(3): p. 231-9.
41. Zhang, X., et al., *Notch1 promotes glioma cell migration and invasion by stimulating beta-catenin and NF-kappaB signaling via AKT activation.* Cancer Sci, 2012. **103**(2): p. 181-90.
42. Wang, Z., et al., *The role of Notch signaling pathway in epithelial-mesenchymal transition (EMT) during development and tumor aggressiveness.* Curr Drug Targets, 2010. **11**(6): p. 745-51.
43. Sahlgren, C., et al., *Notch signaling mediates hypoxia-induced tumor cell migration and invasion.* Proc Natl Acad Sci U S A, 2008. **105**(17): p. 6392-7.
44. Brooks, P.C., et al., *Localization of matrix metalloproteinase MMP-2 to the surface of invasive cells by interaction with integrin alpha v beta 3.* Cell, 1996. **85**(5): p. 683-93.
45. Rao, J.S., et al., *Elevated levels of M(r) 92,000 type IV collagenase in human brain tumors.* Cancer Res, 1993. **53**(10 Suppl): p. 2208-11.
46. Welm, B., J. Mott, and Z. Werb, *Developmental biology: vasculogenesis is a wreck without RECK.* Curr Biol, 2002. **12**(6): p. R209-11.
47. Correa, T.C., et al., *Downregulation of the RECK-tumor and metastasis suppressor gene in glioma invasiveness.* J Cell Biochem, 2006. **99**(1): p. 156-67.
48. Silveira Correa, T.C., et al., *RECK-mediated inhibition of glioma migration and invasion.* J Cell Biochem, 2010. **110**(1): p. 52-61.
49. Tian, Y., H. Wan, and G. Tan, *Cell cycle-related kinase in carcinogenesis.* Oncol Lett, 2012. **4**(4): p. 601-606.
50. Ng, S.S., et al., *Cell cycle-related kinase: a novel candidate oncogene in human glioblastoma.* J Natl Cancer Inst, 2007. **99**(12): p. 936-48.
51. Yang, Y., N. Roine, and T.P. Makela, *CCRK depletion inhibits glioblastoma cell proliferation in a cilium-dependent manner.* EMBO Rep, 2013. **14**(8): p. 741-7.
52. Baldin, V., et al., *Cyclin D1 is a nuclear protein required for cell cycle progression in G1.* Genes Dev, 1993. **7**(5): p. 812-21.
53. Giese, A., et al., *Dichotomy of astrocytoma migration and proliferation.* Int J Cancer, 1996. **67**(2): p. 275-82.

54. Giese, A., et al., *Migration of human glioma cells in response to tumour cyst fluids.* Acta Neurochir (Wien), 1996. **138**(11): p. 1331-40.
55. Wang, S.D., et al., *EphB2 receptor controls proliferation/migration dichotomy of glioblastoma by interacting with focal adhesion kinase.* Oncogene, 2012. **31**(50): p. 5132-43.
56. McDonough, W., et al., *Altered gene expression in human astrocytoma cells selected for migration: I. Thromboxane synthase.* J Neuropathol Exp Neurol, 1998. **57**(5): p. 449-55.
57. Schiffer, D., et al., *Cell proliferation and invasion in malignant gliomas.* Anticancer Res, 1997. **17**(1A): p. 61-9.
58. Moeendarbary, E. and A.R. Harris, *Cell mechanics: principles, practices, and prospects.* Wiley Interdiscip Rev Syst Biol Med, 2014. **6**(5): p. 371-88.
59. Coughlin, M.F., et al., *Cytoskeletal stiffness, friction, and fluidity of cancer cell lines with different metastatic potential.* Clin Exp Metastasis, 2013. **30**(3): p. 237-50.
60. Benitez, R. and J.L. Toca-Herrera, *Looking at cell mechanics with atomic force microscopy: experiment and theory.* Microsc Res Tech, 2014. **77**(11): p. 947-58.
61. Costa, K.D., *Single-cell elastography: probing for disease with the atomic force microscope.* Dis Markers, 2003. **19**(2-3): p. 139-54.
62. Oberleithner, H., et al., *Differential action of steroid hormones on human endothelium.* J Cell Sci, 2006. **119**(Pt 9): p. 1926-32.
63. Rotsch, C. and M. Radmacher, *Drug-induced changes of cytoskeletal structure and mechanics in fibroblasts: an atomic force microscopy study.* Biophys J, 2000. **78**(1): p. 520-35.
64. Titushkin, I. and M. Cho, *Modulation of cellular mechanics during osteogenic differentiation of human mesenchymal stem cells.* Biophys J, 2007. **93**(10): p. 3693-702.
65. Wang, J.H. and B. Li, *Application of cell traction force microscopy for cell biology research.* Methods Mol Biol, 2009. **586**: p. 301-13.
66. Wang, J.H. and J.S. Lin, *Cell traction force and measurement methods.* Biomech Model Mechanobiol, 2007. **6**(6): p. 361-71.
67. Schoen, I., et al., *Probing cellular traction forces by micropillar arrays: contribution of substrate warping to pillar deflection.* Nano Lett, 2010. **10**(5): p. 1823-30.
68. Legant, W.R., et al., *Measurement of mechanical tractions exerted by cells in three-dimensional matrices.* Nat Methods, 2010. **7**(12): p. 969-71.
69. Kraning-Rush, C.M., J.P. Califano, and C.A. Reinhart-King, *Cellular traction stresses increase with increasing metastatic potential.* PLoS One, 2012. **7**(2): p. e32572.
70. Indra, I., et al., *An in vitro correlation of mechanical forces and metastatic capacity.* Phys Biol, 2011. **8**(1): p. 015015.
71. Ohnishi, T., et al., *A novel model of glioma cell invasion using organotypic brain slice culture.* Cancer Res, 1998. **58**(14): p. 2935-40.
72. Garg, K. and G.L. Bowlin, *Electrospinning jets and nanofibrous structures.* Biomicrofluidics, 2011. **5**(1): p. 13403.
73. Vasita, R. and D.S. Katti, *Nanofibers and their applications in tissue engineering.* Int J Nanomedicine, 2006. **1**(1): p. 15-30.
74. Ruckh, T.T., et al., *Osteogenic differentiation of bone marrow stromal cells on poly(epsilon-caprolactone) nanofiber scaffolds.* Acta Biomater, 2010. **6**(8): p. 2949-59.
75. Xie, J., et al., *Neurite outgrowth on nanofiber scaffolds with different orders, structures, and surface properties.* ACS Nano, 2009. **3**(5): p. 1151-9.
76. Kievit, F.M., et al., *Aligned chitosan-polycaprolactone polyblend nanofibers promote the migration of glioblastoma cells.* Adv Healthc Mater, 2013. **2**(12): p. 1651-9.
77. Rao, S.S., et al., *Mimicking white matter tract topography using core-shell electrospun nanofibers to examine migration of malignant brain tumors.* Biomaterials, 2013. **34**(21): p. 5181-90.
78. Johnson, J., et al., *Quantitative analysis of complex glioma cell migration on electrospun polycaprolactone using time-lapse microscopy.* Tissue Eng Part C Methods, 2009. **15**(4): p. 531-40.
79. Kim, Y.T., et al., *The role of aligned polymer fiber-based constructs in the bridging of long peripheral nerve gaps.* Biomaterials, 2008. **29**(21): p. 3117-27.
80. Thomas, G., et al., *Measuring the mechanical properties of living cells using atomic force microscopy.* J Vis Exp, 2013(76).

81. Horzum, U., B. Ozdil, and D. Pesen-Okvur, *Step-by-step quantitative analysis of focal adhesions.* MethodsX, 2014. **1**: p. 56-9.
82. Ohgaki, H., et al., *Genetic pathways to glioblastoma: a population-based study.* Cancer Res, 2004. **64**(19): p. 6892-9.
83. Oberheim, N.A., et al., *Uniquely hominid features of adult human astrocytes.* J Neurosci, 2009. **29**(10): p. 3276-87.
84. Nicchia, G.P., et al., *New possible roles for aquaporin-4 in astrocytes: cell cytoskeleton and functional relationship with connexin43.* FASEB J, 2005. **19**(12): p. 1674-6.
85. Munevar, S., Y. Wang, and M. Dembo, *Traction force microscopy of migrating normal and H-ras transformed 3T3 fibroblasts.* Biophys J, 2001. **80**(4): p. 1744-57.
86. Rape, A.D., W.H. Guo, and Y.L. Wang, *The regulation of traction force in relation to cell shape and focal adhesions.* Biomaterials, 2011. **32**(8): p. 2043-51.
87. Li, T., et al., *Loss of vinculin and membrane-bound beta-catenin promotes metastasis and predicts poor prognosis in colorectal cancer.* Mol Cancer, 2014. **13**: p. 263.
88. Campos, B., et al., *Differentiation therapy exerts antitumor effects on stem-like glioma cells.* Clin Cancer Res, 2010. **16**(10): p. 2715-28.
89. Kong, X., et al., *Differentiation therapy: sesamin as an effective agent in targeting cancer stem-like side population cells of human gallbladder carcinoma.* BMC Complement Altern Med, 2014. **14**: p. 254.
90. Piccirillo, S.G., et al., *Bone morphogenetic proteins inhibit the tumorigenic potential of human brain tumour-initiating cells.* Nature, 2006. **444**(7120): p. 761-5.
91. Graf von Keyserlingk, D. and U. Schramm, *Diameter of axons and thickness of myelin sheaths of the pyramidal tract fibres in the adult human medullary pyramid.* Anat Anz, 1984. **157**(2): p. 97-111.
92. Liewald, D., et al., *Distribution of axon diameters in cortical white matter: an electron-microscopic study on three human brains and a macaque.* Biol Cybern, 2014. **108**(5): p. 541-57.
93. Gardel, M.L., et al., *Mechanical integration of actin and adhesion dynamics in cell migration.* Annu Rev Cell Dev Biol, 2010. **26**: p. 315-33.
94. Roca-Cusachs, P., et al., *Micropatterning of single endothelial cell shape reveals a tight coupling between nuclear volume in G1 and proliferation.* Biophys J, 2008. **94**(12): p. 4984-95.
95. MacKay, J.L., A.J. Keung, and S. Kumar, *A genetic strategy for the dynamic and graded control of cell mechanics, motility, and matrix remodeling.* Biophys J, 2012. **102**(3): p. 434-42.
96. Wang, J., et al., *Knockdown of cyclin D1 inhibits proliferation, induces apoptosis, and attenuates the invasive capacity of human glioblastoma cells.* J Neurooncol, 2012. **106**(3): p. 473-84.
97. Yano, S., et al., *Invading cancer cells are predominantly in G0/G1 resulting in chemoresistance demonstrated by real-time FUCCI imaging.* Cell Cycle, 2014. **13**(6): p. 953-60.
98. Kim, D.H. and D. Wirtz, *Focal adhesion size uniquely predicts cell migration.* FASEB J, 2013. **27**(4): p. 1351-61.
99. Iuliano, J.N., et al., *Metastatic bladder cancer cells distinctively sense and respond to physical cues of collagen fibril-mimetic nanotopography.* Exp Biol Med (Maywood), 2015. **240**(5): p. 601-10.